

1 **Carbon dioxide release driven by organic carbon in minerogenic**
2 **salt marshes**

3 Nora Kainz¹, Franziska Raab¹, L. Joëlle Kubeneck^{2,3,4}, Ruben Kretzschmar², Andreas Kappler¹,
4 Prachi Joshi^{1,5*}

Formatted: English (US)

5 ¹ Department of Geosciences, University of Tübingen, Schnarrenbergstrasse 94-96, 72076 Tübingen, Germany

6 ² Department of Environmental Systems Science, ETH Zürich, CHN, Universitätstrasse 16, 8092 Zürich, Switzerland

7 ³ Department of Microbiology, Radboud Institute for Biological and Environmental Sciences, Radboud University,
8 6525 AJ Nijmegen, The Netherlands

9 ⁴ TNO Geological Survey of the Netherlands, PO Box 80015, 3508 TA Utrecht, The Netherlands

10 ⁵ Swiss Federal Institute for Forest, Snow and Landscape Research WSL, Zürcherstrasse 111, 8903 Birmensdorf,
11 Switzerland

12 **Correspondence:* prachi.joshi@wsl.ch

13 **Abstract**

14 Coastal wetlands play an important role in the global carbon cycle by sequestering carbon (referred to as
15 “blue carbon”). At the same time, organic carbon (OC) in the subsurface is decomposed, releasing greenhouse gases
16 (GHGs) such as carbon dioxide (CO₂) and methane (CH₄). To predict how this carbon balance in salt marshes will
17 change under future climate scenarios (e.g., higher temperatures, sea level rise), it is essential to understand the controls
18 on OC decomposition in these systems. Here, we investigated OC turnover and CO₂ release in a minerogenic salt marsh
19 at the Wadden Sea, Germany. We first characterized the porewater and sediment of a pioneer marsh and adjoining
20 intertidal flat to identify key biogeochemical processes. We then performed an in situ experiment by injecting two OC
21 sources (labile (acetate)/complex (humic acid)) and subsequently monitored GHG release over four injection cycles
22 along with subsurface geochemistry. Overall, we found that the microbially mediated CO₂ release was likely limited
23 by OC availability and composition, and electron acceptor availability was unlikely to be the primary limiting factor,
24 as evidenced by the presence of aqueous sulfate (SO₄²⁻) at all tested depths and the lack of detectable CH₄. Following
25 the addition of labile OC, CO₂ release in the pioneer marsh increased by up to 47.4 ± 36.4 % compared to the control,
26 with a generally similar trend in the intertidal flat. The CO₂ release from the complex OC treatment was similar to the
27 control. The results of our work improve understanding of minerogenic salt marsh OC dynamics in temperate zones
28 and enable better prediction of future changes.

Formatted: Font color: Auto

Deleted: Overall, we found that the microbially mediated CO₂ release was limited by OC availability and composition, and not by electron acceptor availability, as evidenced by the presence of aqueous sulfate (SO₄²⁻) at all depths and the lack of CH₄.

Formatted: Font color: Auto

34 1 Introduction

35 Vegetated coastal wetlands, located at the [interface between land and the open sea](#), occur along all continental
36 coastal zones except Antarctica and comprise mangroves, seagrass, and salt marshes (Nellemann et al., 2009; Pendleton
37 et al., 2012; Tan et al., 2025). Salt marshes, including the seaward adjoining intertidal flats, sequester high amounts of
38 carbon primarily in the sediment (McLeod et al., 2011; Nellemann et al., 2009; de Vlas et al., 2013). Globally, around
39 60.4-70 Tg yr⁻¹ of carbon is buried in vegetated salt marshes (Duarte et al., 2005; Nellemann et al., 2009). The
40 sequestration of carbon is disproportional in vegetated coastal areas, with around half of the total organic carbon in
41 ocean sediment (often referred to as “blue carbon”) buried in these areas which only account for 0.2 % of the ocean
42 surface (Duarte et al., 2013; Nellemann et al., 2009). As the rate of carbon input into the sediment exceeds its rate of
43 decomposition (especially for allochthonous carbon), salt marshes are characterized by high carbon sequestration rates
44 (Mueller et al., 2019; Temmink et al., 2022; Van de Broek et al., 2018). Simultaneously, salt marshes release
45 greenhouse gases (GHGs) due to organic carbon (OC) decomposition: carbon dioxide (CO₂) at 0.02-0.24 Pg CO₂ yr⁻¹
46 (Pendleton et al., 2012) and methane (CH₄) at 0.142 ± 0.02 Mg carbon ha⁻¹ yr⁻¹ (Alongi, 2020). Therefore,
47 understanding carbon turnover in coastal wetlands is crucial for predicting how these ecosystems will respond to
48 climate change, [such as temperature increase, sea level rise, and eutrophication of coastal waters](#). This is especially
49 important given the annual 1-2 % loss of salt marshes due to land-use change and their vulnerability to climate impacts
50 (Duarte et al., 2008).

51 In coastal wetlands, microbial respiration pathways couple OC as an electron donor with terminal electron
52 acceptors (TEAs), especially oxygen (O₂), ferric iron (Fe(III)) and sulfate (SO₄²⁻) (Tan et al., 2025; Tobias and
53 Neubauer, 2019). Oxygen, the thermodynamically most favourable TEA, exhibits fluctuating penetration depth into
54 the sediment due to tides, bioturbation or root-mediated O₂ transport (de Beer et al., 2005; Huettel et al., 2014; Maricle
55 and Lee, 2002). In deeper sediment layers, where anoxic conditions can dominate, microorganisms utilize Fe(III), from
56 iron minerals, or SO₄²⁻, which infiltrates the sediment through inundation of seawater, as alternative TEAs (Jørgensen
57 et al., 2019; Tobias and Neubauer, 2019). Upon full depletion of TEAs, OC is further decomposed to CH₄ (Schlesinger
58 and Bernhardt, 2013b). Microbial decomposition of OC may be further influenced by its chemical composition.
59 Chemically simpler e.g., short chain aliphatic OC may be substantially favoured for decomposition compared to
60 complex OC, such as natural organic matter (Gunina and Kuzyakov, 2022; Lipczynska-Kochany, 2018; Schlesinger
61 and Bernhardt, 2013a).

62 The primary controls on GHG release in salt marshes, as interfaces between land and open ocean, are not
63 fully understood. Specifically, it is unclear whether OC turnover is primarily controlled by the availability of the
64 electron acceptors – as observed in organogenic marshes and consistent with studies in terrestrial wetlands (Schlesinger
65 and Bernhardt, 2013b) – or by the organic matter itself, as suggested for marine sediment in general (Arndt et al.,
66 2013). Past studies on OC dynamics (including GHG release) in salt marshes have largely concentrated on the eastern
67 coast of the US (Capooci et al., 2024; Kostka et al., 2002b; Lowe et al., 2000; Seyfferth et al., 2020), which is dominated
68 by organogenic peat marshes. [Organogenic marshes are generally low energy, microtidal wetlands, characterized by a
69 high organic matter deposition via autochthonous pathways that results in high TOC contents](#) (Logemann et al., 2025).
70 For example, Lowe et al. (2000) and Kostka et al. (2002a) observed that OC oxidation was controlled by SO₄²⁻ and

Deleted: intersection

Formatted

Field Code Changed

72 Fe(III) reduction in salt marshes in Georgia, USA. Further, CH₄ fluxes were detected in salt marshes in Delaware,
73 suggesting a co-occurrence of methanogenesis and SO₄²⁻ reduction (Capooci et al., 2024; Seyfferth et al., 2020).
74 European salt marshes, in contrast, are primarily minerogenic, i.e., contain high fractions of mineral sediment due to
75 high sedimentation rates, resulting in comparably lower TOC content (Nolte et al., 2013). Studies conducted in
76 European salt marshes have focused on the TEA turnover (e.g., SO₄²⁻ respiration rates) and not GHG emissions (de
77 Beer et al., 2005; Bosselmann et al., 2003; van Erk et al., 2023). These studies showed that O₂ penetrates down the
78 sediment, Fe(III) is available and SO₄²⁻ reduction occurs. Hence, these studies have provided indirect links between
79 belowground biogeochemistry, especially in the context of available TEA, and the release of GHGs in minerogenic
80 salt marshes; however, a direct investigation of the determining factor(s) of OC degradation from these ecosystems is
81 missing. By understanding the controls on GHG release, we can better predict how climate impacts such as higher
82 temperatures and sea level rise will affect OC turnover and thereby GHG release in minerogenic salt marshes.

Deleted:

83 To investigate the in situ carbon dynamics in minerogenic salt marshes, we chose a representative field site
84 at the Wadden Sea coast. Our goals were (i) to identify the key microbial processes (O₂, Fe(III) and/or SO₄²⁻ reduction)
85 that control the release of OC as CO₂ and/or CH₄, and (ii) to determine the role of OC (concentration and composition)
86 in the release of GHGs. To this end, we first characterised the primary geochemical parameters from a minerogenic
87 pioneer marsh and intertidal flat at the German Wadden Sea. Building on those results, we conducted an in situ
88 manipulation experiment investigating the impact of two contrasting OC sources (acetate, humic acid) on GHG
89 emissions. We hypothesized that (i) the high energy and sediment inputs in minerogenic salt marshes result in low
90 TOC supply and high TEA availability. (ii) We further hypothesize that this leads to the likely limitation of electron
91 donor and not acceptor on OC decomposition and (iii) the composition of OC plays a more important role than the
92 concentration in CO₂ release from a minerogenic salt marsh. These hypotheses were tested in two successional zones
93 of a salt marsh, a pioneer marsh with sparse pioneer vegetation and a non-vegetated intertidal flat.

Deleted: These studies have provided indirect links between belowground biogeochemistry and the release of GHGs in minerogenic salt marshes; however, a direct investigation of the determining factor(s) of OC degradation from these ecosystems is missing

Deleted: Building on those results, we conducted an in situ manipulation experiment investigating the impact of two contrasting OC sources (acetate, humic acid) on GHG emissions from a minerogenic pioneer marsh and intertidal flat...

105 **2 Materials and Methods**

106 **2.1 Study site**

107 This study was conducted at the Altfelder Koog by Friedrichskoog (54°01'02.4"N 08°51'17.09"E), an area
108 that consists of a salt marsh with different successional zones in the Wadden Sea National Park (Schleswig-Holstein)
109 in northern Germany at the mouth of the Elbe estuary (Fig. 1a). The Wadden Sea is a UNESCO World Heritage Site
110 and the largest continuous salt marsh (including tidal flats) in Europe (Common Wadden Sea Secretariat, 2017). The
111 tidal range at the study area is 3.59 m, defined as the difference between mean height of high water and approximately
112 the lowest astronomical tide. The mean high tide is 1.56 m higher than the mean sea level (BSH, 2025).

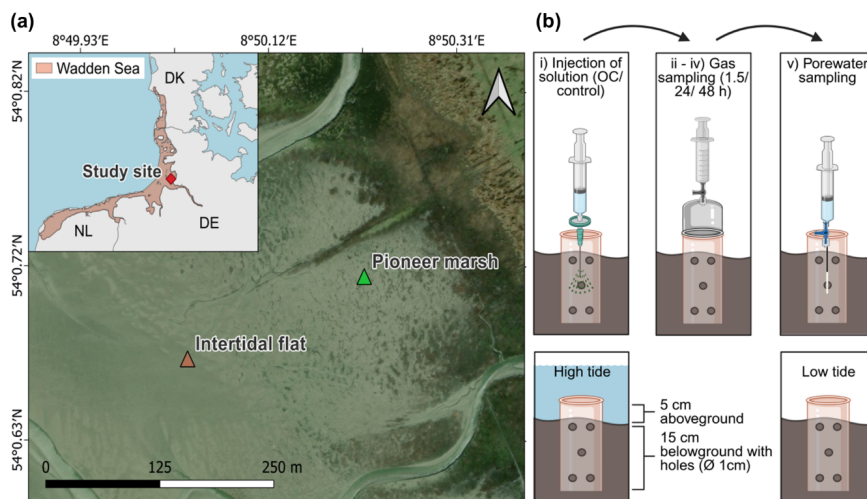
113 At the Wadden Sea, different successional zones of salt marshes are developing as a result of the ongoing
114 process of sediment transportation by waves and tides (Esselink et al., 2017; de Vlas et al., 2013). The two successional
115 zones which are of interest in our study are the pioneer marsh and the intertidal flat (Fig. 1a). Pioneer species such as
116 *Salicornia* spp. and *Spartina anglica* occur in the pioneer marsh, promoting further sediment trapping (Esselink et al.,
117 2017; de Vlas et al., 2013). The intertidal flat (seaward of a pioneer marsh) is an area with no plants to buffer incoming
118 waves and is therefore subject to a strong tidal influence (Esselink et al., 2017). In general, both the pioneer marsh and
119 intertidal flat are inundated daily during high tide, with the pioneer marsh experiencing less and shorter inundation (<
120 3 h fully inundated) compared to the intertidal flat (> 3 h fully inundated) (de Vlas et al., 2013). During a spring tide,
121 which occurs twice a month, the magnitude of high and low tide is amplified leading to stronger exposure of the pioneer
122 marsh to tides (Gao, 2019; Kvale, 2006).

Deleted: B

Deleted: twice a day

Deleted:

Deleted: high tide



127

128 **Figure 1. Study site at the Wadden Sea including the successional zones of a salt marsh and a schematic representation of**
 129 **the in situ experimental design.** (a) Wadden Sea, in light red in the inset with a red marker indicating our study site in northern
 130 Germany (Friedrichskoog, Elbe estuary). Gradient of salt marsh succession zones, beginning with the intertidal flat, followed by
 131 the pioneer marsh and more developed successional zones extending further inland. Map information: Reference system WGS 1984,
 132 UTM 32N, data imagery ESRI 2025. (b) Experimental design: experimental procedure (top) and cylinder setup in sediment (below).
 133 Each sampling plot consisted of a 20 cm long cylinder (diameter 16 cm), drilled with 1 cm diameter holes along the length of the
 134 cylinder. The cylinder was inserted 15 cm deep in the sediment to define the injection area. The top 5 cm was used to mount a gas
 135 chamber during gas sampling. The cylinder stayed in the sediment over the course of the experiment including high and low tide.
 136 Numbers i-v indicate the experimental procedure: i) injection of solution (acetate or humic acid, only NaCl for control), ii) 1.5 h
 137 after injection, the first gas measurement was done, iii) followed by the second gas measurement after 24 h of injection, and iv) the
 138 final gas measurement after 48 h of injection, followed by the final step of v) porewater sampling. Each treatment (acetate, humic
 139 acid) and the control consisted of spatial triplicates.

140 2.2 Porewater and sediment sampling for general geochemistry

141 In August 2022 and 2023, sediment cores were collected from the pioneer marsh and intertidal flat to analyse
 142 the general geochemistry of the sediment and porewater. The sampling was performed during low tide. Push cores
 143 were collected using core liners (UWITEC, polyvinyl chloride PVC) with an inner diameter of 8.6 cm (outer diameter
 144 9 cm) and a length of 60 cm. [To minimize compression, we used open push cores and only capped them when the core](#)
 145 [liner was fully in the sediment. Furthermore, the inside wall of the cores was plain and clean to smoothly insert the](#)
 146 [core liner in the sediment. To further minimize disturbance, the sampled cores were immediately closed, vertically](#)
 147 [transported, and stored in the dark.](#) At depth intervals of 5 cm, porewater samples (Rhizon sampler CSS, 0.12-0.18 μ m
 148 pore size, Rhizosphere Research, Netherlands) and sediment samples (using a cut-off syringe) were taken through
 149 pre-drilled holes which had been covered with isolation tape during coring. [We made sure to not take sediment or](#)

150 [porewater samples at the edges but rather from the middle of the cores, where the sediment is likely undisturbed.](#)
151 Porewater samples were analysed for dissolved organic carbon (DOC), iron speciation, SO_4^{2-} , and dissolved CH_4 , and
152 sediment samples for total organic carbon (TOC). Detailed method for dissolved CH_4 sampling is given in Supplement,
153 S1.1.

154 We collected further sediment cores for fine scale O_2 profiles. For this, sediment push cores (inner diameter
155 2.5 cm, length 10 cm) were collected and immediately sealed. Shortly after sampling, O_2 profiles were taken with a
156 depth resolution of 500 μm using Clark-type O_2 microsensors (Unisense, Denmark) with a 100 μm tip, following
157 Revsbech (1989). Before measurement, a two-point calibration was done using air-saturated seawater and 0.1 M
158 sodium ascorbate in 0.1 M NaOH solution. Profiles were recorded with the Unisense software SensorTrace Suite
159 (version 2.8.200.21688, Unisense, Denmark).

160 2.3 Physicochemical characteristics of the sediment

161 For a general physicochemical characterization, bulk sediment was collected from a depth up to 15-20 cm in
162 sterile sample bags with puncture proof tabs (Nasco, Whirl-pak, USA), and stored at 4 °C in the dark. Stones and
163 macrofauna were removed prior to further analysis. We determined grain density, bulk porosity, moisture content, and
164 particle size (details in Supplement, S1.2).

165 2.4 In situ experiment: Enhanced organic carbon input

166 2.4.1 In situ experiment design

167 An in situ OC addition experiment was conducted in August and September 2023 to test the response of
168 pioneer marsh and intertidal flat systems to elevated inputs of OC with different compositions. We choose acetate, a
169 chemically simple organic compound that has been detected at other salt marshes (Hyun et al., 2007; Kostka et al.,
170 2002a) and at a site nearby (Llobet-Brossa et al., 2002), and humic acid (in the form of Pahokee Peat humic acid), a
171 more complex OC source, as a proxy for natural organic matter. The two OC sources were chosen, knowing their
172 thermodynamical difference from previous studies (Gunina and Kuzyakov, 2022), to present a fermentation product
173 (acetate) and a proxy for terrestrial organic matter (in addition to the difference with respect to complexity). [Studying](#)
174 [both labile and complex OC additions is ecologically relevant as salt marshes receive OC from multiple sources](#)
175 [\(Howard et al., 2023; Temmink et al., 2022\). Eutrophication of coastal waters and/or root exudates can supply readily](#)
176 [degradable OC to salt marshes, while increased organic matter load in rivers can deliver more complex OC compounds](#)
177 [to salt marshes. The applied OC compounds in our study, therefore, represent environmental scenarios and allows us](#)
178 [to investigate how these OC sources influence GHG release under realistic conditions.](#) The injection solutions were
179 prepared in the laboratory prior to use in the field. Solutions of 1 g OC L^{-1} were prepared with either acetate or humic
180 acid as a carbon source. For the preparation of the solutions, sodium acetate or Pahokee Peat humic acid (obtained
181 from the International Humic Substances Society (IHSS), Table S1) were dissolved in deionized water (Barnstead MQ
182 system, Thermo Fisher Scientific, Germany), the pH was adjusted to 7.07-7.81 and NaCl was added (20 g L^{-1}). The
183 solution for the control only contained NaCl. Additionally, 25 mM bromide (Br^-) (in the form of NaBr) was added into

Deleted:

185 the carbon and control solutions as an inert tracer in the field. All solutions were purged with nitrogen and stored at 4
186 °C in the dark until used in the field. Details of the preparation process are provided in Supplement, S1.3.

187 The in situ experiment was performed in the pioneer marsh (54°00'43.14"N 08°50'12.9"E) and intertidal flat
188 (54°00'40.45"N 08°50'02.27"E) (Fig. 1a), with the same setup in both zones. The assigned plots in the field were
189 selected as visually similar triplicates (spatial triplicates), at a distance of ~5 m between plots of the same treatment
190 and ~10 m between different treatments and the control plots. In the pioneer marsh, plots were placed outside of
191 vegetated areas, i.e., the actual plot area of injection and sampling were free of vegetation although vegetation was
192 present in the vicinity (Figs. S1a/b). For the intertidal flat, no vegetation was present, neither in the surroundings nor
193 inside of the plots (Figs. S1c/d). Each plot consisted of a 16 cm diameter PVC cylinder with both ends open which
194 was pushed 15 cm deep into the sediment (Fig. 1b). Holes (diameter 1 cm) were drilled in the cylinder wall to allow
195 underground water movement. A porewater sampler (Rhizon sampler CSS, 0.12-0.18 µm pore size, Rhizosphere
196 Research, Netherlands) was inserted in the middle of each plot at a depth of 5-10 cm and remained in the sediment
197 over the duration of the experiment. The cylinder reached 5 cm out of the sediment, allowing a gas flux chamber to be
198 mounted gastight for gas measurements. During the experiment, the cylinder stayed in the field. To decrease the
199 influence of disturbances due to the setup of the experiment, we waited at least three days between setting up and the
200 first measurements. Apart from the incubation time for gas sampling, the sediment within the cylinder was exposed to
201 the atmosphere (low tide) or covered with seawater (high tide) (Fig. 1b).

202 The experiment was conducted similarly in both zones, the pioneer marsh and intertidal flat, using spatial
203 triplicates and comprising four injection cycles (Fig. 1b). One injection cycle consisted of i) the injection of the anoxic
204 sterile solution (OC or control solution), followed by ii) the first gas sampling 1.5 h after the injection. Gas sampling
205 was repeated iii) 24 h after the injection and iv) 48 h after the injection. After the 48 h gas sampling, v) porewater was
206 collected. Injection of the solutions and sampling was done during low tide. The solution for the different treatments
207 was slowly injected in step i) with a bent needle at a depth of approximately 5-10 cm in the middle of each plot into
208 the sediment. The injected solution was filtered (PES filter, pore size 0.22 µm, pre-rinsed with double deionized water)
209 during injection to ensure that the solutions were sterile.

210 In each injection cycle, the native OC was increased by 12.0 mg C L⁻¹ in the pioneer marsh and 12.6 mg C L⁻¹
211 in the intertidal flat, assuming an even distribution across the experimental cylinder (calculation Supplement, S1.4).
212 After one cycle was completed, the system had three days to recover before the next injection. At the end of the four
213 injection cycles, sediment samples were collected (details below). [The applied approach allowed us to assess short-](#)
214 [term OC process response in minerogenic salt marshes, rather than long-term responses.](#)

215 2.4.2 In situ experiment sampling

216 Gas sampling

217 Gas sampling was conducted using an opaque, static, non-flow gas chamber made of polypropylene ([chamber](#)
218 [volume 3000 cm³](#)). The gas chamber was placed on the cylinder and gas samples were collected at 20-minute intervals
219 over an incubation period of 1 hour using a 50 mL gastight syringe with a three-way valve. For sampling, the chamber

220 gas was gently mixed by pumping the syringe plunger three times before withdrawing 35 mL gas. The first 5 ml were
221 used to flush the attached needle, and the rest was transferred immediately into a pre-evacuated 12 mL Exetainer® vial
222 (Labco, UK). The samples were measured with a Greenhouse GC equipped with two Pulsed Discharge Detector (PDD)
223 (ThermoFisher Scientific TRACE™ 1310 GC-Analyzer, USA – custom designed by S+H-Analytik) and two column
224 structure (first structure 30 m long, 0.53 mm ID TGBondQ column, second structure 30 m long, 0.53 mm ID Molsieve
225 column (for CH₄) and 30 m long 0.32 mm ID TGBondQ+ column (for CO₂, N₂O)). Calculation for the gas fluxes and
226 cumulative CO₂ emissions are given in Supplement, S1.5.

227 **Porewater sampling**

228 Porewater samples were collected via the pre-installed porewater sampler. The pH (Mettler Toledo SevenGo,
229 Germany) and salinity (refractometer) were measured in the field. The collected porewater was fixed for DOC
230 (acidification with 2 M HCl), iron speciation (acidification with 1 M HCl), and total sulfide (S(II)_{tot}) (alkalinization
231 with zinc acetate). Dissolved inorganic carbon (DIC) samples were transferred into vials without headspace
232 immediately after sampling and capped. The remaining porewater was anoxically stored in nitrogen flushed bottles in
233 the dark at 4 °C for Br⁻, SO₄²⁻ and chloride (Cl⁻) measurements.

234 **Sediment sampling**

235 At the end of the experiment, sediment samples were collected for geochemical analysis (TOC, solid iron
236 speciation, sulfide species) and microbial analysis. For this, push cores (inner diameter of 2.5 cm, and a length 10 cm)
237 were taken from the middle of each plot at the same positions as the porewater samples and immediately frozen until
238 further analysis. Sediment samples for the molecular biology analysis were stored at -80 °C upon bringing them back
239 to the laboratory.

240 **2.5 Geochemical analysis**

241 **2.5.1 Porewater analysis**

242 DOC (as non-purgeable OC) and DIC (as the difference of total carbon and OC) was determined by a TOC
243 analyser (multi N/C 2100S, Analytik Jena GmbH, Germany). To analyse the iron speciation in the porewater, the
244 ferrozine assay (Stookey, 1970) was used. The S(II)_{tot} was quantified by the Cline assay (Cline, 1969). Sulfate, Br⁻,
245 and Cl⁻ were analysed by an ion chromatograph (Metrohm 930 Compact IC Flex, Switzerland).

246 **2.5.2 Sediment analysis**

247 For all sediment analyses, sampled cores were thawed in an anoxic glovebox to prevent oxidation (UNILab
248 plus Glovebox, MBRAUN, Germany), sliced in two depths (0-5 and 5-10 cm), and each depth fraction was
249 homogenized by hand.

250 **Iron extraction**

251 To target the poorly and higher crystalline iron phases in the sediment samples, parallel iron extractions were
252 performed under anoxic conditions, adapted from Moeslund et al. (1994) and Lueder et al. (2020). From each depth

253 (0-5 and 5-10 cm) ~0.2 g wet sediment sample (in triplicates) were added into an Eppendorf tube. To extract poorly
254 crystalline iron minerals, we used an extraction with anoxic 0.5 M HCl (Heron et al., 1994). We expect that poorly
255 crystalline iron (oxyhydr)oxides as well as ferrous iron (Fe(II)) phases such as carbonates and sulfides (e.g., FeCO₃ or
256 FeS) would be extracted by this acidification. One mL of anoxic 0.5 M HCl was added to the sediment, vortexed, and
257 incubated for 2 h in the dark at room temperature in the glovebox. For the extraction of iron minerals of higher
258 crystallinity, targeting more crystalline Fe(II) (except pyrite) and Fe(III) phases (Cornwell and Morse, 1987; Heron et
259 al., 1994), 1 mL of anoxic 6 M HCl was added to the sediment, and the sediment was vortexed and vertically rotated
260 for 24 h under anoxic conditions at room temperature (30 rpm, dark). For both HCl extractions, the samples were then
261 centrifuged (5 min, 13400 rpm), the supernatant was diluted with 1 M HCl, and iron speciation and concentration of
262 the supernatant was determined using the ferrozine assay (Stookey, 1970). Total iron and Fe(II) concentrations of the
263 supernatant were measured directly, and Fe(III) was determined by subtracting Fe(II) from total iron. To obtain the
264 higher crystalline fraction separately, the poorly crystalline fraction (0.5 M HCl extract) was subtracted from the 6 M
265 HCl fraction. [We acknowledge that the weaker acid extraction extracted Fe\(II\) from carbonates and sulfides in addition
266 to iron \(oxyhydro\)oxides. We therefore used this approach to determine the crystallinity of iron minerals and call it
267 poorly \(extracted by 0.5 M HCl\) and higher \(extracted by 6 M HCl\) crystalline iron minerals \(and not \(oxyhydr\)oxides\).](#)

268 **Acid volatile sulfide**

269 To determine the mass of acid volatile sulfide (AVS) in the sediment similar to Burton et al. (2007), ~2 g of
270 wet sediment was weighed in centrifuge tube in a glovebox. A smaller tube filled with anoxic 1 M zinc acetate + anoxic
271 2 M NaOH (v/v 15:85) was placed into the sediment-filled centrifuge tube. To the sediment, 10 mL anoxic 6 M HCl
272 + 2 mL anoxic 1 M L-ascorbic acid was added and immediately closed. The double tubes were placed in an ultrasonic
273 bath for 30 seconds, followed by horizontal shaking overnight (150 rpm). The sulfide released from the sediment was
274 captured in the zinc acetate solution and was analysed according to Cline (1969).

275 **Total organic carbon**

276 To quantify sediment TOC, samples collected in 2023 were dried under anoxic conditions, while those from
277 2022 were dried under oxic conditions, at room temperature until constant weight was reached. Sediments from both
278 years were milled and analysed by a TOC analyser (SoliTOC Cube Elementar, Germany).

279 **2.6 Molecular biology analysis**

280 The co-extraction of DNA and RNA was performed according to Lueders et al. (2004). Quantitative
281 polymerase chain reaction (qPCR) for DNA and complementary DNA (cDNA) was done to quantify total bacterial
282 16S rRNA gene copies using the primer 341F and 797R. Functional genes were also targeted: *Geobacter* spp. (involved
283 in Fe(III) reduction) using the primer Geo 577F and Geo 822R, and *dsrA* (involved in SO₄²⁻ reduction) using the primer
284 DSR_1F and DSR_1R. Quantitative polymerase chain reaction was done using SsoAdvanced SYBR Green Supermix
285 (Bio-Rad) on the C1000 Touche Thermal Cycler (CFX96™ Real-Time System, Bio-Rad, Germany). Data analysis
286 was performed by the software Bio-Rad CFX Maestro 1.1 (version 4.1.2433.1219). Further details are given in
287 Supplement, S1.6 and Table S2.

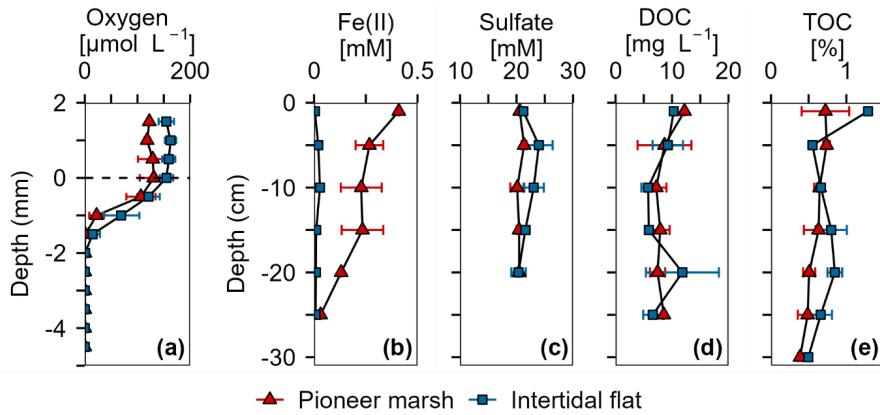
288 **2.7 Statistical analysis**

289 For statistical analysis RStudio (R version R-4.4.3) was used. The significance level for all tests was set at p
290 < 0.05. Normal distribution of the data and homogeneity of variances were tested by Shapiro-Wilk test and Levene
291 test, respectively. Correlations between parameters was tested with the relevant tests (Pearson's correlation test or
292 Spearman's rank correlation test depending on the normality of the data). Statistical differences between two groups
293 were tested with a t-test and for more than two groups with a one-way Analysis of Variance (ANOVA) or Kruskal-
294 Wallis rank sum test. For differences in the CO₂ release, a linear mixed model was applied. More details on the chosen
295 tests and model are given in Supplement, S1.7. We reported the p-value in the text; further relevant statistical test
296 results and parameters are shown in the corresponding sections in the SI. The variability of the geochemistry analysis
297 is represented by the standard deviation of triplicates/duplicates. For the in situ experiment, the variability is reflected
298 in the standard error of triplicates. For duplicate analyses, variability reflects the range of the two samples.

Deleted: For statistical analysis RStudio (R version R-4.4.3) was used. The significance level for all tests was set at p < 0.05. More details on the chosen tests are given in Supplement, S1.7. We reported the p-value in the text; further relevant statistical test results are shown in the corresponding sections in the SI.

305 **3 Results**

306 **3.1 Geochemistry at the study site**



307

308 **Figure 2. Overview of porewater and sediment biogeochemistry in terms of electron acceptors (O_2 , Fe(III), SO_4^{2-}) and**
309 **electron donor (DOC, TOC) from in situ push cores in the pioneer marsh (red triangles) and intertidal flat (blue squares).**
310 (a) Oxygen concentration profiles measured in intact cores using microsensors. Note that these cores were collected in 2022, separate
311 from the push cores used for analysis shown in (b-e). Two cores were collected from each zone and two to four profiles were taken
312 from each core, shortly (within hours) after sampling. (b) Ferrous iron in the porewater, as an indicator of Fe(III) reduction. (c)
313 Sulfate concentrations in the porewater. (d) Dissolved organic carbon in the porewater. (e) Total organic carbon in the sediment.
314 For (b-d), push cores were taken in triplicates in both zones to a depth of 25 cm in 2023. Duplicate push cores for (e) the TOC were
315 sampled in 2022. For all sub-figures, markers denote mean \pm standard deviation (due to limited sample mass, some depth values
316 only show mean and the range of two samples, or only a single value). All cores were sampled during low tide.

317 Porewater and solid phase measurements from the push and microsensor cores analysis show availability of
318 electron acceptors (O_2 , Fe(III), and SO_4^{2-}) over depth in both the pioneer marsh and intertidal flat (Fig. 2). In the pioneer
319 marsh, O_2 decreased from $131.02 \pm 26.49 \mu\text{mol L}^{-1}$ at the sediment-water interface to $0.18 \pm 0.12 \mu\text{mol L}^{-1}$ over 2 mm
320 and was depleted beyond this depth. We observed a similar trend for the intertidal flat, with $155.17 \pm 12.71 \mu\text{mol L}^{-1}$
321 at the sediment-water interface, and a decrease to $0.62 \pm 1.10 \mu\text{mol L}^{-1}$ at 2 mm depth before it was fully depleted (Fig.
322 2a). Aqueous Fe(II) (as an indicator of Fe(III) reduction) showed a decreasing trend in both zones, with higher
323 concentration in the pioneer marsh of $267.49 \pm 66.77 \mu\text{M}$ at 5 cm depth and $31.41 \mu\text{M}$ at 25 cm, and 19.93 ± 16.15
324 μM at 5 cm decreasing to $7.20 \pm 2.89 \mu\text{M}$ at 25 cm in the intertidal flat (Fig. 2b). Sulfate was detected in the porewater
325 at all sampled depths (1.5 to 20 cm) in both zones (Fig. 2c). In the pioneer marsh, it ranged in the upper 20 cm from a
326 minimum of 20.12 ± 1.23 to a maximum of $21.34 \pm 0.43 \text{ mM}$ and in the intertidal flat from 20.35 ± 1.27 to $23.95 \pm$
327 2.44 mM . We observed a slight decrease in SO_4^{2-} concentration over depth which was more pronounced in the intertidal
328 flat. This is further supported by the ratio of sulfate:chloride (Fig. S2a). The ratio remained constant in the pioneer
329 marsh, while a slight decrease was measured in the intertidal flat. We also measured SO_4^{2-} at lower depths (up to 50

Deleted: grey

Deleted: (e) Total organic carbon in the sediment.

Deleted: We measured concentrations of Fe(II) as an indicator of Fe(III) reduction.

334 cm) in cores taken in 2022 and observed similar SO_4^{2-} concentrations (Fig. S2b). To complement the porewater Fe(II),
335 we measured the 0.5 M HCl extractable Fe(III) from the bulk sediment from a depth up to 15-20 cm: $1.30 \pm 1.08 \mu\text{mol}$
336 Fe(III) g^{-1} dry sediment in the pioneer marsh and $1.00 \pm 0.51 \mu\text{mol}$ Fe(III) g^{-1} dry sediment in the intertidal flat. The
337 resulting Fe(II) to total iron ratio was 0.98 ± 0.02 and 0.98 ± 0.01 respectively.

338 Organic carbon as the likely electron donor was measured in the porewater as non-purgeable organic carbon
339 and in the sediment as TOC. The DOC and TOC decreased slightly over depth (Fig. 2d/e) in both zones. In the pioneer
340 marsh, the DOC was $12.21 \text{ mg C L}^{-1}$ at the top (1 cm deep) and decreased over depth to 8.55 mg C L^{-1} at 25 cm. For
341 the intertidal flat, the DOC at the top (1 cm deep) was $10.31 \text{ mg C L}^{-1}$ and decreased to $6.60 \pm 1.69 \text{ mg C L}^{-1}$ at 25 cm.
342 The TOC decreased from $0.7 \pm 0.3 \%$ at the top to $0.5 \pm 0.1 \%$ at a depth of 25 cm in the pioneer marsh and from 1.3%
343 to $0.7 \pm 0.2 \%$ in the intertidal flat (Fig. 2e). Concentrations at lower depths are shown in Supplement, Fig. S2c, and
344 are in a similar range. [In both the pioneer marsh and intertidal flat, no \$\text{CH}_4\$ release, neither as fluxes or in the porewater](#)
345 [up to a depth of 50 cm, was detected \(detection limit: 0.28 and 0.53 ppm respectively; Table S3\).](#)

346 Particle size analysis indicated that sediment from the pioneer marsh was dominated by fine particles, whereas
347 the intertidal flat sediment was coarser. In the sediment of the pioneer marsh, we determined $41.7 \pm 9.1 \%$ sand,
348 $38.7 \pm 2.5 \%$ silt, and $19.7 \pm 8.1 \%$ clay. For the sediment of the intertidal flat, a higher sand fraction ($61.5 \pm 0.5 \%$),
349 less silt ($29.0 \pm 5.0 \%$), and notably lower clay content ($9.5 \pm 5.5 \%$) was measured. For more details on the size
350 fractions, see Supplement, Table S4.

351 3.2 In situ organic carbon manipulation experiment

352 3.2.1 Distribution of bromide tracer and dissolved organic carbon in the sediment

353 Bromide was used in the in situ experiment as an inert tracer to test the washing out of the injection solution
354 from the experimental plot over the sampling time of one injection cycle (48 h). The native Br^- concentration was
355 $0.66 \pm 0.02 \text{ mM}$ in the pioneer marsh and $0.63 \pm 0.01 \text{ mM}$ in the intertidal flat. Assuming an equal distribution of the
356 injected solution in the experimental cylinder, we expected the Br^- concentration to increase by 0.30 mM to a final
357 concentration of 0.99 mM in the plots of the pioneer marsh and by 0.32 mM to a final concentration of 0.97 mM for
358 the plots in the intertidal flat (calculations Supplement, S1.4 – expected Br^- concentration). Throughout a test injection
359 cycle with the same sampling intervals as the experimental injection cycles, the Br^- concentration remained above the
360 background level with a gradual decrease over time in both zones (Figs. S3a/b). Overall, after 48 h (one injection
361 cycle), Br^- levels in the porewater remained elevated in each cycle for both zones. In the pioneer marsh, an average of
362 $77.5 \pm 5.9 \%$ of the expected level of Br^- remained in the porewater of the experimental cylinder. The intertidal flat
363 had a slightly lower average residual fraction of $72.1 \pm 4.4 \%$ of the expected Br^- level across all injection cycles (Fig.
364 3). [Here, residual fraction is defined as the ratio between the \$\text{Br}^-\$ concentration measured in the porewater 48 h post](#)
365 [injection and the expected total \$\text{Br}^-\$ concentration in an experimental cylinder \(Eq. \(1\); details in S1.4\). The expected](#)
366 [total \$\text{Br}^-\$ concentration includes both the native \$\text{Br}^-\$ and the added \$\text{Br}^-\$ during the experiment \(expected \$\text{Br}^-\$ \) after](#)
367 [accounting for dilution in the sediment. Details on the calculation of the \$\text{Br}^-\$ residual fraction are provided in](#)
368 [Supplement, S1.4.](#)

Deleted: In both the pioneer marsh and intertidal flat, no CH_4 release, neither as fluxes or in the porewater up to a depth of 50 cm, was detected in 2022.

Deleted: 3

Deleted: simplified,

374

$$\frac{\text{Br}^- \text{ concentration at the end of an injection cycle}}{\text{Br}^- \text{ expected}} = \text{residual fraction} \quad (1)$$

375

The residual fraction of DOC is defined in the same way as for Br⁻, representing the proportion of measured DOC after 48 h to the expected DOC (native DOC + added acetate/humic acid) and was calculated analogously to Br⁻, with DOC concentrations used instead (Eq. (1) and S1.4).

377

Comparing the average residual fraction of DOC and Br⁻ (Fig. 3) across all injection cycles, the DOC fraction was significantly lower in both the pioneer marsh and intertidal flat (Br⁻ vs. acetate and Br⁻ vs. humic acid) ($p \leq 0.001$, Table S5).

378

In the pioneer marsh, $40.0 \pm 1.2\%$ of the injected DOC in the acetate treatment remained, on average across all injection cycles, while the corresponding value for the humic acid treatment was $52.9 \pm 4.5\%$.

380

In the intertidal flat, relatively less carbon remained, with a smaller difference between the carbon sources. Here, the mean residual fraction was $38.2 \pm 4.8\%$ for the acetate treatment and $37.3 \pm 3.6\%$ for the humic acid treatment.

383

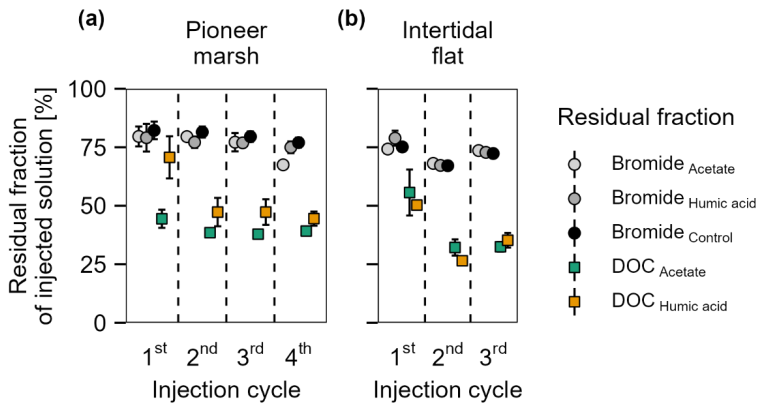
Deleted: The term residual fraction here refers to the ratio of Br⁻ concentration measured in the porewater 48 h post injection (end of an injection cycle) to the expected total concentration in an experimental cylinder, which includes both native and added Br⁻ (expected Br⁻). Details on the calculation of the Br⁻ residual fraction are provided in Supplement, S1.4.

Deleted: The residual fraction of DOC is defined in the same way, representing the proportion of measured DOC after 48 h to the expected DOC (native DOC + added acetate/humic acid) and was calculated in the same way as for Br⁻ (Supplement, S1.4).

Deleted: 4

Deleted: for the

Formatted: Font color: Text 1, English (US)



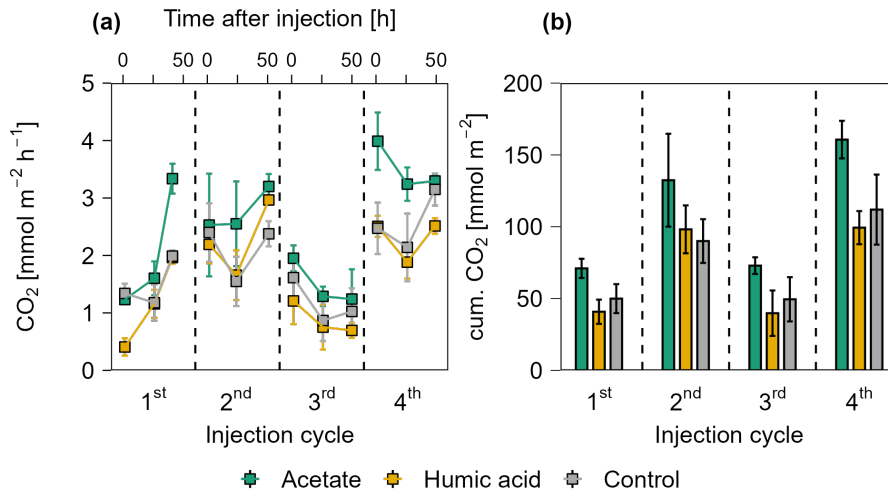
384

399 **Figure 3. Residual fraction of injected solutions (Br⁻ and DOC) in percentage after 48 h for treatments (acetate, humic acid)**
400 **and control plots in the (a) pioneer zone (over four injection cycles) and (b) intertidal flat (over three injection cycles).**
401 Coloured squares show the residual fraction of injected DOC (acetate in green and humic acid in orange). The grey shaded circles
402 represent the residual of Br⁻ from the different treatments and the control. The values were calculated based on the ratio between
403 the measured DOC or Br⁻ concentration (porewater concentration 48 h post injection) and the expected DOC or Br⁻ concentration
404 (native + added). Markers represent the mean of the triplicates, with error bars indicating the corresponding standard error for
405 treatments and control in both zones for DOC and Br⁻ across all injection cycles.

Deleted: The markers represent the mean of the triplicates, and the error bars indicate the standard error.

408 3.2.2 Effect of organic carbon input in the pioneer marsh

409 Carbon dioxide release



410

411 **Figure 4.** CO₂ release over four OC injection cycles for the acetate, humic acid, and control plots in the pioneer marsh. The
 412 dashed lines separate the individual injection cycles. (a) presents individual measured CO₂ fluxes 1.5, 24, and 48 h after injection
 413 in CO₂ mmol m⁻² h⁻¹. Acetate (green), humic acid (orange), and NaCl for the control (grey) were injected into the sediment and
 414 GHG fluxes were measured directly above the injection spot at the aforementioned time intervals. (b) shows the cumulative CO₂
 415 emissions in CO₂ mmol m⁻² over one injection cycle for each treatment and control. We note here that some variability in the fluxes
 416 based on factors such as day/night could not be captured in our sampling approach; we therefore aimed to use a consistent approach
 417 and report relative changes rather than emphasize absolute values. For (a/b), markers represent mean ± standard error of triplicates
 418 for all treatments and the control across injection cycles. For the 1st and 3rd injection cycle for the acetate treatment (both 1.5 h
 419 values) were based on duplicate measurements, which is thus also the case for the (b) cumulative CO₂ emission of these cycles.

420 **Figure 4** presents the CO₂ release for each injection cycle with the individual CO₂ fluxes 1.5, 24, and 48 h
 421 post injection (Fig. 4a) and the cumulative CO₂ emissions (Fig. 4b) in the pioneer marsh. For all four injection cycles,
 422 the CO₂ fluxes of the acetate treated plots exceeded the CO₂ fluxes of the humic acid and control plots (Fig. 4a). For
 423 the first injection cycle, the acetate treatment was significantly higher compared to the humic acid treatment ($p < 0.05$,
 424 Table S6) and slightly above the threshold for statistical significance ($p = 0.08$, Table S6) compared to the control. In
 425 the following injection cycle, the CO₂ fluxes of the acetate treatment were also higher compared to the humic acid and
 426 control plots but not significantly ($p > 0.05$). Hence, the acetate treated plot consistently exhibited the highest fluxes.
 427 The difference between the humic acid and control plots was statistically negligible ($p > 0.05$). Similarly, the
 428 cumulative CO₂ emissions from the acetate treated plots were the highest while the emissions from the humic acid and

Deleted: Markers represent triplicates: mean ± standard error.

Deleted: (mean ± standard error)

Deleted: Figure 4

Formatted: Font: 10 pt, Not Bold

Formatted: Font: 10 pt, Not Bold, Not Italic, Check spelling and grammar

Deleted: 5

Deleted: 5

Deleted: Complementarily

436 control plots were in a similar range for all four injection cycles (Fig. 4b). The CO₂ emitted from the acetate treated
437 plots was up to 83.2 ± 53.7 % higher than for the humic acid treated plots. Similarly, the emissions of the acetate plots
438 were up to 47.4 ± 36.4 % higher relative to the control plots. No statistical differences were measured between the
439 cumulative CO₂ emission of the acetate treated plots and the control or humic acid treatment. Overall, these differences
440 were smaller than those seen at individual CO₂ fluxes at specific time points (Fig. 4a), likely due to high variability in
441 fluxes that resulted in variable cumulative CO₂ emissions. In all treatments and the control, no CH₄ as a flux was
442 detected (lower than detection limit (0.28 ppm); Table S3).

Deleted: In all treatments and the control, no CH₄ was detected.

443 The CO₂ fluxes showed a positive correlation with air temperature and a moderate positive correlation with
444 the tidal cycle in the pioneer marsh (Table S7). Specifically, CO₂ fluxes were found to be higher as the spring tide
445 receded. Lower CO₂ fluxes were measured during the first and third injection cycles, which occurred close to spring
446 tides.

Deleted: 6

447 Further differences between the treatments and control were observed in the DOC concentrations (Fig. S4)
448 and the residual fraction of DOC (Fig. 3a) in the pioneer marsh. Over all four injection cycles, the average DOC
449 concentration in the acetate treated plots did not significantly differ from the control ($p > 0.05$), while the DOC
450 concentrations of the humic acid treated plots were significantly higher than the concentrations of acetate treated plots
451 and the control plots ($p < 0.05$, Table S8). These differences are consistent with the residual fraction of DOC (Fig. 3a).
452 Across all four injection cycles, the average residual fraction in the humic acid treatment was significantly higher
453 compared to the acetate treatment but significantly lower than the Br⁻ residual fraction ($p < 0.002$, $p < 0.001$
454 respectively, Table S5). No difference in the TOC content was found between treatments and control in both depths.
455 The content ranged from 0.9 ± 0.1 % to 1.2 ± 0.1 % in the upper 5 cm, with a slight decrease at lower depth (Table S9).

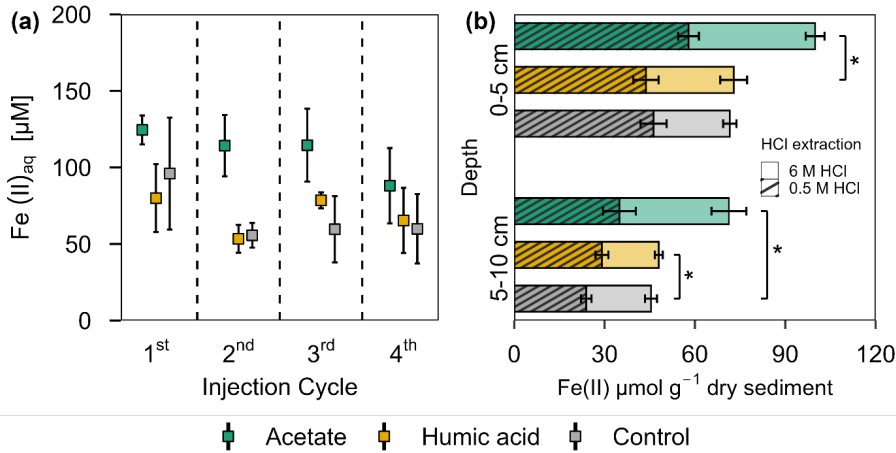
Deleted: 7

Deleted: 4

Deleted: 8

456 In addition to the gas fluxes, we also measured DIC and pH of the porewater for each treatment and control
457 for each injection cycle (Fig. S5). As the differences in the CO₂ fluxes were more pronounced and our focus was on
458 GHG release, we only present and later discuss these data.

465 Effect of organic carbon input on the geochemistry of porewater and sediment



466 Acetate Humic acid Control
 467 **Figure 5. Ferrous iron in (a) porewater and (b) solid phase from acetate and humic acid treated plots and the control plots**
 468 **in the pioneer marsh.** (a) Aqueous ferrous iron (Fe(II)_{aq}) [µM] sampled after each injection cycle (cycles are separated by the
 469 dashed line). Triplicates for each treatment and control [for each injection cycle](#) were collected and mean ± standard error is shown.
 470 (b) HCl extractable Fe(II) content [µmol g⁻¹ dry sediment] at two different depths (0-5 and 5-10 cm) sampled at the end of all four
 471 injection cycles. Different colour coding was used for contrasting treatments: acetate treatment (green), humic acid treatment
 472 (orange), and control (grey). Striped bars represent poorly crystalline Fe(II) (0.5 M HCl extraction) and solid bars higher crystalline
 473 Fe(II) (6 M HCl extraction). The 0.5 M HCl extract was subtracted from the 6 M HCl extracted fraction to separate poorly and
 474 higher crystalline Fe(II). [Significance is denoted for the 0.5 M HCl extraction. Statistical details are given in the SI \(Table S11\).](#)
 475 [significance level p < 0.05 *.](#) [For each treatment and control, each spatial triplicate \(n = 3\) was analyzed in triplicate \(total n = 9\)](#)
 476 [for each depth \(0-5 and 5-10 cm\); results are presented as mean ± standard error.](#)

Deleted: Each spatial triplicate was analysed in triplicates; results are presented as means ± standard error.

477 In the pioneer marsh, acetate treated plots had significantly higher aqueous Fe(II) concentrations compared
 478 to humic acid and control plots when considering the average concentration across all injection cycles (acetate vs.
 479 humic acid p = 0.007 and vs. control p = 0.002, Table S10). Although the differences were not always statistically
 480 significant for the individual cycles, the Fe(II) concentration in the porewater of the acetate treated plots was
 481 consistently higher (Fig. 5a): 1st cycle 124.52 ± 9.44 µM, 2nd cycle 114.20 ± 19.98 µM, 3rd cycle 114.54 ± 23.80 µM,
 482 and 4th cycle 88.08 ± 24.58 µM. Humic acid treated plots and the control plots showed similar aqueous Fe(II)
 483 concentrations. For humic acid treated plots the aqueous Fe(II) concentration ranged between 53.36 ± 9.05 µM
 484 (2nd cycle) and 79.96 ± 22.16 µM (1st cycle), and for the control between 55.69 ± 8.04 (2nd cycle) and 96.01 ± 36.61
 485 µM (1st cycle) (Fig. 5a).

Deleted: 9

486 A similar trend can be seen in the solid phase for the HCl extractable Fe(II), for both extractions approaches
 487 (0.5 M and 6 M HCl) (Fig. 5b). Comparing the poorly crystalline Fe(II) fraction, the acetate treatment had the highest

Deleted: We are aware that the weaker acid extraction extracted Fe(II) from carbonates and sulfides in addition to iron(oxyhydro)oxides. We therefore used this approach to determine the crystallinity of iron minerals and call it poorly (extracted by 0.5 M HCl) and higher (extracted by 6 M HCl) crystalline iron minerals (and not (oxyhydr)oxides).

497 Fe(II) content compared to the humic acid treatment and the control at both depths. Acetate treated plots showed an
498 Fe(II) content of $57.87 \pm 3.44 \mu\text{mol g}^{-1}$ sediment in the upper 5 cm and $34.91 \pm 5.45 \mu\text{mol g}^{-1}$ sediment from 5-10 cm.
499 Humic acid and control plots had similar levels of Fe(II): for the humic acid plots, the content in the upper 5 cm was
500 $43.74 \pm 4.18 \mu\text{mol g}^{-1}$ sediment and from 5-10 cm, it was $29.13 \pm 2.12 \mu\text{mol g}^{-1}$ sediment. The control plots showed
501 $46.28 \pm 4.32 \mu\text{mol g}^{-1}$ sediment in the upper 5 cm and $23.93 \pm 1.75 \mu\text{mol g}^{-1}$ sediment between 5 to 10 cm. We observed
502 the same trend for the higher crystalline Fe(II) content. The acetate treatment had the highest contents with 42.04 ± 3.12
503 $\mu\text{mol g}^{-1}$ sediment (0-5 cm) and $36.38 \pm 5.79 \mu\text{mol g}^{-1}$ sediment compared with humic acid or control plots. For both
504 depth and crystallinities, the acetate treatment showed significantly the highest content, in nearly all comparisons to
505 the humic acid or control plots (Table S11). Except for poorly crystalline Fe(II) at 5-10 cm depth, humic acid and
506 control plots did not differ significantly (Table S11).

507 No consistent difference was detected in $S(\text{II})_{\text{tot}}$ in the porewater of the pioneer marsh (Fig. S6a). The $S(\text{II})_{\text{tot}}$
508 concentrations were in the same range: acetate from $3.16 \pm 0.01 \mu\text{M}$ (4th cycle) to $5.59 \pm 1.21 \mu\text{M}$ (1st cycle), humic
509 acid from $3.0 \pm 0.11 \mu\text{M}$ (4th cycle) to $6.34 \pm 1.56 \mu\text{M}$ (1st cycle) and control from $3.63 \pm 0.34 \mu\text{M}$ (1st cycle) to
510 $4.39 \pm 1.13 \mu\text{M}$ (4th cycle). Also, statistical analysis did not reveal a difference between the different treatments and
511 control $S(\text{II})_{\text{tot}}$ averaged over all cycles ($p > 0.05$). Similarly, AVS measurements of the solid sulfide species showed
512 no difference between treatments and the control (Fig. S6b). In the upper 5 cm, contents were similar (acetate:
513 6.13 ± 1.40 , humic acid 3.89 ± 1.19 , and control $7.37 \pm 1.76 \mu\text{mol g}^{-1}$ sediment). Similar contents were measured at
514 5-10 cm depth, with no coherent trend between the layers.

515 Effect of organic carbon input on microbial growth and metabolic activity

516 The impact of the added OC on the bacterial community was analysed by qPCR. The analyses were based on
517 DNA (microbial abundance) and RNA (metabolically active microorganisms). The results show the gene copies of
518 both treatments normalized to the control as \log_2 fold change ($\log_2 \text{FC}$) (Fig. 6). Statistics are based on the absolute
519 gene copy numbers (Fig. S7). For the acetate treated plots a significantly higher bacterial 16S rRNA gene copy number
520 (DNA- and RNA-based) was measured compared to the control plots across all analysed depths (Fig. 6a; $p < 0.05$). In
521 comparison to the control, DNA-based bacterial 16S rRNA gene copies increased by a factor of 0.4 ± 0.07 ($\log_2 \text{FC}$)
522 under acetate treatment and their potential activity, indicated by RNA, increased by $1.58 \pm 1.46 \log_2 \text{FC}$ in the upper 5
523 cm. This remained similar at the depth of 5-10 cm, with an increase in DNA-based 16S rRNA gene copies by $0.43 \pm$
524 $0.09 \log_2 \text{FC}$ and an increase in activity (RNA) by $5.09 \pm 1.86 \log_2 \text{FC}$. For the comparison between plots amended
525 with humic acid and the control, variations were observed but no significant differences were measured ($p > 0.05$).
526 Microbial activity (RNA) of *Geobacter* spp., were higher in the acetate and humic acid treatment compared to the
527 control in the upper 5 cm, however, slightly over the significance criterion (Fig. 6b; $p = 0.051$, $p = 0.057$, respectively).
528 For the acetate treated plots, the activity (RNA-based) of *Geobacter* spp. was higher compared to the control by a
529 factor of 0.98 ± 0.49 . The humic acid treatment also had upregulated activity by a factor of 0.72 ± 0.31 . The higher
530 microbial activity of *Geobacter* spp. remained significantly enhanced ($p = 0.008$) for the acetate treatment compared
531 to the control at the lower depth (RNA-based: $\log_2 \text{FC}$: 0.66 ± 0.15), too. The addition of OC did not affect the microbial
532 activity (RNA) of *dsrA* genes at both depths (Fig. 6c) in the pioneer marsh. However, the abundance (DNA) of *dsrA*

Deleted: 0

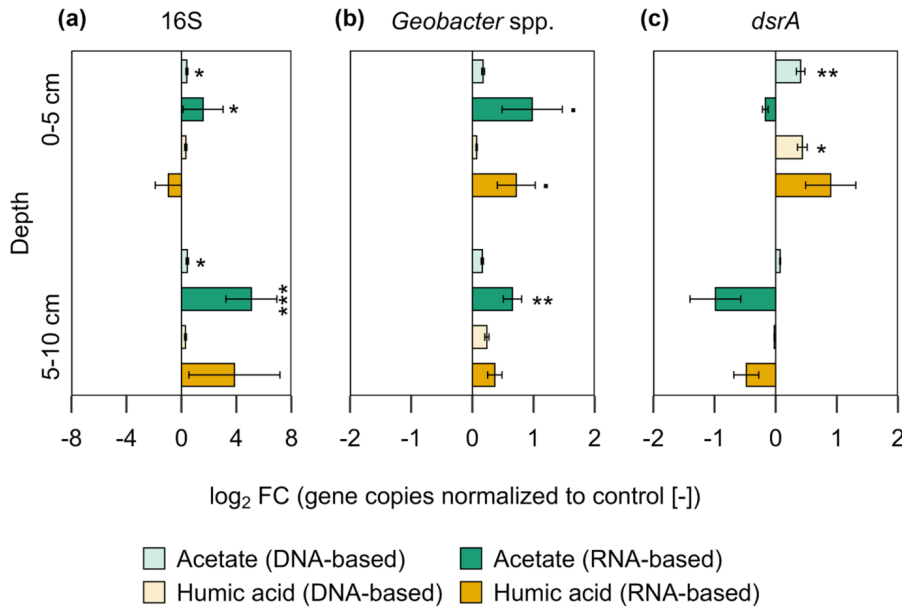
Deleted: 0

Deleted: Overall, a decreasing trend from higher contents in the upper 5 cm to lower contents in the deeper layer (5-10 cm) was notable for all treatments and crystallinities.

Deleted: to quantify the total bacterial abundance (bacterial 16S rRNA gene copy numbers), the abundances of *Geobacter* spp. as an indicator for Fe(III) reduction, and the *dsrA* gene as an indicator for sulfate-reducing bacteria (SRB) in the pioneer marsh.

543 genes in the upper layer was significantly higher for both treatments (acetate $p = 0.006$, humic acid $p = 0.015$). Absolute
 544 gene copy numbers are given in Supplement, Fig. S7 and statistical details in Table S12.

Deleted: 1

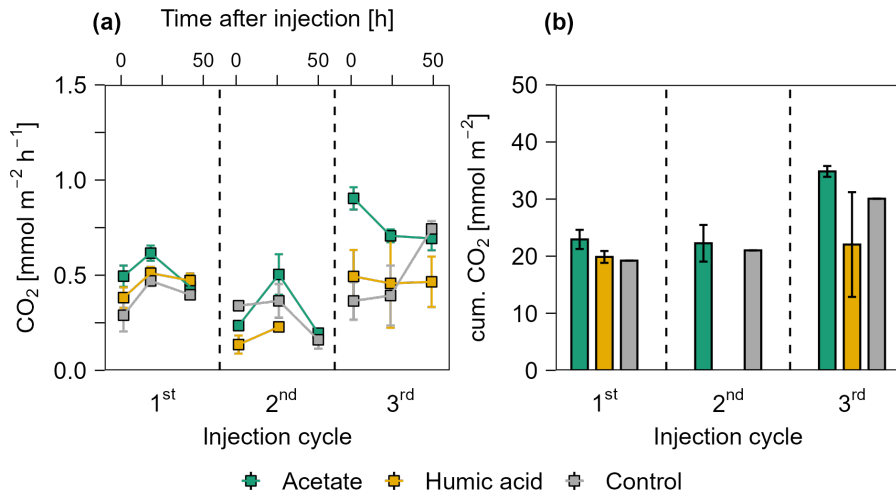


545
 546 **Figure 6. Bacterial gene copy numbers of (a) 16S rRNA (16S), (b) *Geobacter* spp., and (c) *dsrA* for acetate and humic acid**
 547 **treatment normalized to the control in the pioneer marsh.** The values are represented as log₂ fold change (FC). Values > 0
 548 indicate an upregulation while values < 0 indicate downregulation of the genes compared to the control (acetate in green, humic
 549 acid in orange). DNA-based numbers are given in lighter colours and RNA-based in darker colours. Statistical differences in the
 550 absolute gene copy numbers are indicated as stars in the figure: significant codes are $p = 0.05$., $p \leq 0.05$ *, $p \leq 0.01$ **, and
 551 $p \leq 0.001$ ***. Absolute gene copy numbers given in Supplement, Fig. S7. [Sample sizes include triplicates of each treatment and](#)
 552 [control at both depths, represented as mean ± standard error \(exception of duplicate measurements for 16s RNA-based humic](#)
 553 [substances \(5-10 cm\) and 16s RNA-based control \(0-5 cm\)\).](#)

Deleted: Sample sizes include triplicates, represented as mean ± standard error.

557 3.2.3 Effect of organic carbon input in the intertidal flat

558 Carbon dioxide release



559

560 **Figure 7.** CO₂ release over three injection cycles for the acetate and humic acid treated plots and the control plots in the
 561 intertidal flat. (a) CO₂ fluxes after 1.5, 24, and 48 h after injection in CO₂ mmol m⁻² h⁻¹ over three injection cycles. The dashed
 562 lines separate the individual injection cycles. In the 2nd injection cycle, fluxes in the humic acid treatment are only displayed at 1.5
 563 and 24 h post injection due to missing data. Acetate (green), humic acid (orange), and NaCl for the control (grey) were injected into
 564 the sediment and GHG fluxes were measured directly above the injection spot at the aforementioned time intervals. (b) presents the
 565 cumulative CO₂ release in mmol CO₂ m⁻² over one injection cycle for each treatment and control. Due to missing values for humic
 566 acid amended plots in the second injection cycle, cumulative emissions could not be calculated. For the same reason, standard errors
 567 of the control plots are also not available. For (a/b), markers represent the mean ± standard error of triplicates for all treatments and
 568 the control across injection cycles, except where missing values for CO₂ release occurred due to nonlinear CO₂ release during the
 569 gas sampling incubation time. (a) duplicate measurements are reflected for the 1st injection cycle for the control (1.5 and 24 h), for
 570 the 2nd injection cycle for the acetate treatment and control (48 h), and the 3rd injection cycle for the acetate treatment and control
 571 (1.5, 24, and 48 h). Single measurement values are shown for the control in the 1st (48 h) and 2nd (1.5 h) injection cycle. For (b),
 572 cumulative CO₂ emissions, the acetate treatment shows duplicate measurements for the 2nd and 3rd injection and for the control,
 573 only single values are reflected.

574 Figure 7a presents the CO₂ release from the intertidal flat over three injection cycles 1.5, 24, and 48 h post
 575 injection. Acetate treated plots released the highest CO₂ in all three injection cycles compared to the humic acid and
 576 the control plots. Similar to the pioneer marsh, no strong differences were observed between humic acid treated plots
 577 and the control plots. Consistently, the maximum cumulative CO₂ emissions were observed in the acetate treated plots
 578 (Fig. 7b). Due to nonlinearity of CO₂ release over the incubation time of gas sampling, some data points are missing;

Deleted: Markers represent triplicates: mean ± standard error....

Deleted: Figure 7

Formatted: Font: 10 pt, Not Bold

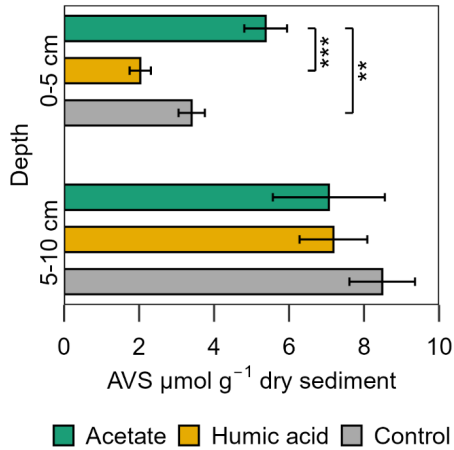
Formatted: Font: 10 pt, Not Bold, Not Italic, Check spelling and grammar

582 therefore, statistical comparison of CO₂ release between treatments and the control was not done. Nevertheless, plots
 583 amended with acetate consistently showed higher CO₂ releases across all injection cycles. Methane was not detected
 584 in the fluxes of any treatment in the intertidal flat plots (lower than detection limit (0.28 ppm); Table S3). Similar to
 585 the pioneer marsh, we focus here on CO₂ data although DIC and pH were measured (Fig. S8).

586 No difference in the DOC concentrations between the treatments and the control were measured (Fig. S9).
 587 Similarly, no difference was measured between the residual fraction (recovery of injected DOC) between acetate and
 588 humic acid treatments (Fig. 3b). The TOC content among the treatments and the control was also in the same range
 589 (0.4-0.5 %) (Table S9).

590 **Effect of organic carbon input on the geochemistry of porewater and sediment**

591 In the intertidal flat, aqueous Fe(II) concentrations ranged from 9.25 ± 0.21 to 24.82 ± 4.50 μM in both
 592 treatments and the control, with no significant differences (p > 0.05) (Fig. S10a). Additionally, no difference between
 593 the treatments and the control was detected in the solid phase for both crystallinities (0.5 and 6 M HCl extraction) and
 594 depths. In the upper 5 cm, the content of the poorly crystalline Fe(II) ranged from 18.28 ± 1.28 to 19.60 ± 0.88 μmol g⁻¹
 595 sediment among all treatments and control, while in the deeper layer, the range was from 18.11 ± 0.71 to 24.59 ± 1.22
 596 μmol g⁻¹ sediment. The content of the higher crystalline Fe(II) ranged from 11.68 ± 0.99 to 20.06 ± 3.64 μmol g⁻¹
 597 sediment in the upper 5 cm and from 12.98 ± 1.03 to 17.50 ± 2.75 μmol g⁻¹ sediment at a depth of 5-10 cm (Fig. S10b).



598
 599 **Figure 8. Acid volatile sulfide (AVS) in the solid phase sampled at the end of the experiment for the acetate and humic acid**
 600 **treated plots and the control plots in the intertidal flat.** AVS [μmol g⁻¹ dry sediment] content of the solid phase from the different
 601 treatments (acetate in green, humic acid in orange) and control (grey). Significance is denoted for the upper sediment layer (0-5
 602 cm), deeper layer no statistically significant difference occurred. Statistical details are given in the SI (Table S13), significance level

Deleted: were not possible

Deleted: Acetate treated plots released the highest CO₂ in all three injection cycles compared to the humic acid and the control plots, with significantly higher CO₂ fluxes compared to the humic acid treatment in the second injection cycle (p = 0.04, Table S12). Similar to the pioneer marsh, no significant differences were observed between humic acid treated plots and the control plots (p > 0.05). Consistently, the maximum cumulative CO₂ emissions were observed in the acetate treated plots (Fig. 7b).

Deleted: Methane was not measured in the fluxes of any treatment in the intertidal flat plots.

Deleted: 8

616 $p < 0.05$ *, $p < 0.01$ **, and $p < 0.001$ ***. Each spatial triplicate ($n=3$) was analyzed in triplicates (total $n = 9$) for each treatment
617 and the control at both depths; results are presented as mean \pm standard error.

Deleted: Each spatial triplicate was analysed in duplicates; results are presented as means \pm standard error.

618 For porewater $S(II)_{tot}$, no large differences were measured between the treatments and control in the intertidal
619 flat. The concentrations of both treatments and the control were in a similar range over all injection cycles, 0.62 ± 0.01
620 to $1.73 \pm 0.67 \mu M S(II)_{tot}$ (Fig. S11). In contrast, the AVS in the solid phase exhibited a significant difference between
621 the treatments and the control (Fig. 8). Higher AVS contents were measured in the acetate plots. This difference was
622 strongly pronounced in the upper 5 cm in the acetate plots relative to the setups amended with humic acid and the
623 control ($p < 0.001$ and $p = 0.007$, respectively, Table S13). AVS content in the upper 5 cm was $5.38 \pm 0.57 \mu mol g^{-1}$
624 sediment from the acetate plots, $2.03 \pm 0.28 \mu mol g^{-1}$ sediment from the humic acid plots, and $3.40 \pm 0.35 \mu mol g^{-1}$
625 sediment from the control. In the deeper layer (5-10 cm), the differences between treatments and control were
626 statistically negligible ($p > 0.05$).

Deleted: ¶

627 Effect of organic carbon input on microbial growth and metabolic activity

628 In the intertidal flat, an increase in DNA- and RNA-based gene copy numbers of the bacterial 16S rRNA gene
629 was detected in the acetate treatment compared to the control at both depths (0-5 and 5-10 cm) (Fig. S12a). This
630 increase was significant for DNA and RNA in the upper layer and remained significant for RNA in the lower layer (p
631 = 0.008, $p = 0.01$, and $p = 0.008$, respectively). The acetate treatment showed a $3.62 \pm 2.41 \log_2 FC$ increase in the
632 metabolic activity (RNA) of the total microbial community compared to the control in the upper layer and an increase
633 of $2.73 \pm 1.41 \log_2 FC$ from 5-10 cm. For *Geobacter* spp. (Fig. S12b) the RNA-based gene copies were significantly
634 higher compared to the control ($p < 0.001$) by a factor of 0.6 ± 0.10 in the upper 5 cm. No significant increase in the
635 RNA-based copy numbers of *dsrA* genes in both depths (Fig. S12c) were observed; however, we detected slightly
636 higher RNA-based *dsrA* gene copies in the acetate treatments ($0.33 \pm 0.06 \log_2 FC$) compared to the control in the
637 upper layer. Absolute gene copy numbers are presented in Fig. S13 and statistical details in Table S14.

Formatted: Font: Italic

Deleted: The addition of neither acetate nor humic acid caused a significant increase in the RNA-based copy numbers of *dsrA* genes in both depths (Fig. S12c). However, we detected slightly higher RNA-based *dsrA* gene copies in the acetate treatments ($0.33 \pm 0.06 \log_2 FC$) compared to the control in the upper layer.

649 4 Discussion

650 4.1 Geochemistry at the study site

651 Porewater and solid phase measurements from the push cores showed availability of electron acceptors (O₂,
652 Fe(III), and SO₄²⁻) at different depths in both the pioneer marsh and intertidal flat. Based on microsensor measurements
653 during low tide, we observed O₂ concentrations in the top 2 mm decreasing with depth, from 131.02 ± 26.49 to 0.18 ±
654 0.12 μmol L⁻¹ in the pioneer marsh, and in the intertidal flat from 155.17 ± 12.71 to 0.62 ± 1.10 μmol L⁻¹, reaching 0
655 μM below that depth. This finding directly affects which biogeochemical processes occur below this depth. Other
656 studies conducted in comparable ecosystems have indicated that during high tide and/or daytime, O₂ penetrates deeper
657 into the sediment (de Beer et al., 2005; Bosselmann et al., 2003), but reducing conditions may prevail underneath and
658 that the depth of O₂ penetration might be influenced by sediment grain size. Both zones in our study showed a high
659 proportion of fine particles (silt: 29.0 ± 5.0 to 38.7 ± 2.5 % and clay: 9.5 ± 5.5 to 19.7 ± 8.1 %). Such a size distribution
660 retains more water (Novák and Hlaváčiková, 2019), resulting in water-filled pore spaces even during low tide, which
661 limits gas exchange. We suggest that the lack of O₂ penetration beyond 2 mm at our study site results from the presence
662 of fine particles. Despite differences in the duration and magnitude of inundation between the zones, the depth of O₂
663 penetration remained similar, indicating that these factors do not influence O₂ penetration depth and that reducing
664 conditions prevail beyond the upper millimetres during both tidal conditions. We do not exclude that the presence of
665 sparse vegetation in the pioneer marsh compared to no vegetation in the intertidal flat may cause differences in the
666 intrusion of O₂ into the sediment (Koop-Jakobsen et al., 2017; Maricle and Lee, 2002). However, we did not detect
667 this difference in our O₂ measurements. In addition to plants, benthic organisms such as worms may introduce O₂ into
668 the sediment and influence the biogeochemical cycling in the sediment (Huettel et al., 2014). As worms were present
669 in both zones, it is likely that they play a role in O₂ penetration and re-oxidizing of reduced Fe(II) or sulfide species
670 (Figs. S14a-d). We expect that this effect is not substantially different for the two zones, as no large qualitative
671 difference in the presence of worms was observed visually. ▲

672 Below the oxic zone, alternative electron acceptors were present. We used Fe(II) porewater data as an
673 indicator of Fe(III) reduction. A decrease in the aqueous Fe(II) from 267.49 ± 66.77 to 31.41 μM Fe(II) in the pioneer
674 marsh and from 19.93 ± 16.15 to 7.20 ± 2.89 μM Fe(II) in the intertidal flat was measured over 25 cm. Based on the
675 presence of aqueous Fe(II), we assumed that Fe(III) reduction is likely occurring in both zones, which is less
676 pronounced in the intertidal flat. The observed decreasing trend over depth has been commonly seen in other studies
677 of coastal sediment (Moeslundi et al., 1994; Lowe et al., 2000). It suggests a depletion of bioavailable Fe(III) with
678 depth and/or removal of aqueous Fe(II). Aqueous Fe(II) can precipitate with sulfide, which forms through SO₄²⁻
679 reduction deeper in the sediment when more thermodynamically favourable electron acceptors are exhausted
680 (Jørgensen et al., 2019). The Fe(II) porewater concentrations are in the range of other studies from salt marshes,
681 especially for the pioneer marsh (0-800 μM) (Kostka et al., 2002b; Seyfferth et al., 2020). Concentrations of the
682 intertidal flat are on the lower end of the studies mentioned above. Ferrous iron was the predominant iron species in
683 the solid fraction extracted by 0.5 M HCl in both zones. Manganese(IV) as an electron acceptor was not further
684 considered as the total manganese concentration from the study site is 5 μmol g⁻¹ sediment (Kubeneck et al., 2025),
685 and thus relatively low in comparison to the total iron concentration.

Deleted: Based on microsensor measurements during low tide, we observed O₂ in the top 2 mm, decreasing to 0 mM below. This suggests that reducing conditions were present below 2 mm during low tide.

Deleted: speculate

Formatted: Font: (Default) +Body (Calibri), 11 pt, Font color: Text 1, English (US)

691 Sulfate has a major role in the oxidation of OC as an important electron acceptor in coastal wetlands due to
692 its frequent supply via the incoming seawater. We observed a slight decrease in SO_4^{2-} over a depth of 20 cm which
693 was more distinct in the intertidal flat, as seen in the sulfate to chloride ratio (Fig. S2a). This suggests some SO_4^{2-}
694 reduction in the upper 20 cm. A similar pattern was observed at a comparable site where Fe(II) predominates over total
695 iron and porewater SO_4^{2-} concentration decreases with depth, albeit with slightly higher SO_4^{2-} concentrations (Kostka
696 et al., 2002b). The relatively high levels of SO_4^{2-} at all tested depths (>50 cm), supported the absence of detectable
697 CH_4 dissolved in the porewater or as an efflux. This is consistent with past studies such as Martens and Berner (1974)
698 who stated that if more than ~10 % of seawater SO_4^{2-} is still present, CH_4 is not produced, as a thermodynamically
699 more favourable electron acceptor is available (Schlesinger and Bernhardt, 2013b). We examined different possible
700 explanations for the lack of detected CH_4 as we could not entirely exclude that CH_4 was produced further down in the
701 sediment and oxidized via anaerobic methane oxidation (AOM), as observed in some coastal wetlands (Capooci et al.,
702 2024; La et al., 2022; Wang et al., 2019), or by lateral transport to surrounding tidal channels (Trifunovic et al., 2020).
703 We did not measure any CH_4 as an efflux or in the porewater over multiple field campaigns, similar to a study conducted
704 at the same study site by Kubeneck et al. (2025). Furthermore, the absence of an observed decrease in SO_4^{2-}
705 concentration, particularly in the pioneer marsh, suggest a lack of AOM until 50 cm, as CH_4 and SO_4^{2-} are consumed
706 in a 1:1 stoichiometric ratio during sulfate AOM. The few other studies that have detected CH_4 in the Wadden Sea were
707 at depths where SO_4^{2-} was largely depleted (Roy et al., 2008; Wu et al., 2015), which is not the case in our study. Thus,
708 our results indicate that CH_4 production and consumption is unlikely until 50 cm, and could occur, if at all, below these
709 depths. Further analysis using microbial analysis and/or CH_4 injection experiments is needed to fully exclude
710 methanogenesis and AOM at lower depths. Collectively, due to the occurrence of Fe(III) reduction (especially in the
711 upper sediment layers) and the availability of SO_4^{2-} throughout the sediment, we suggest that electron acceptor
712 availability likely did not limit microbial OC decomposition in our study.

713 We also considered the OC sources in the system: porewater DOC and solid phase TOC. The TOC content
714 was ~1 % and decreased with depth in both zones. A decreasing trend over depth was also seen in the DOC
715 concentrations. The decrease of OC with depth indicates decomposition and has been commonly observed in other
716 studies (Hansen et al., 2017; Mueller et al., 2019). The range in TOC and DOC concentrations are at the lower end of
717 comparable ecosystems with the main differences in the upper centimetres (Gribsholt and Kristensen, 2003; Hansen et
718 al., 2017; Mueller et al., 2023).

719 Based on the availability of electron acceptors (e.g., SO_4^{2-}) at all depths and the lack of detectable CH_4 , we
720 hypothesize that at our field site and other comparable coastal sites, OC is likely the constraint on microbially mediated
721 CO_2 release and that electron acceptors are likely not a limiting factor. To our knowledge, this is rarely reported for
722 coastal wetlands and not commonly expected for terrestrial ecosystems. Hence, we performed an in situ experiment to
723 test this hypothesis.

724 4.2 In situ organic carbon manipulation experiment

725 4.2.1 Validation of the experimental setup

Deleted: (

Deleted: .

Deleted: assume

Deleted: Collectively, these results indicate that electron acceptors (especially SO_4^{2-}) were available throughout the sediment and therefore, electron acceptor availability did not limit microbial OC decomposition in our study.

Deleted: Based on the availability of electron acceptors (i.e., SO_4^{2-}) at all depths and the lack of CH_4 , we hypothesize that at our field site and other comparable coastal sites, OC is the likely constraint on microbially mediated CO_2 release and that electron acceptors are not a limiting factor.

738 Bromide, as an inert tracer, was injected along with the OC/control solution into each experimental cylinder
739 for each injection cycle. This allowed us to follow the distribution and retention time of the injected solution over one
740 injection cycle. The Br⁻ concentration over each injection cycle was higher than the background Br⁻ concentration (Fig.
741 3/S3a/b), indicating that the injected solution was partially retained within the experimental cylinder over one injection
742 cycle. The observed decrease in Br⁻ concentration over one injection cycle, more pronounced in the intertidal flat (Fig.
743 S3b), was likely due to flushing out by tidal water and belowground water movement. We observed a slightly lower
744 retention of Br⁻ in the intertidal flats compared to the pioneer zone. We attribute this difference to the higher sand
745 fraction in the intertidal flats, which likely increased permeability and led to stronger tidal flushing of the injected
746 solution as well as subject to greater tidal inundation.

747 As the Br⁻ concentrations and the respective calculated residual fractions were similar for each cycle (Fig. 3),
748 we infer that there was no residue of Br⁻ and thus no injected OC was carried over between cycles. Furthermore, the
749 retained Br⁻ was similar between the plots of a treatment within one zone, indicating similar belowground conditions
750 within one zone and thereby validating the experimental setup. By placing the experimental plots outside of vegetated
751 areas in the pioneer marsh, we tried to avoid geochemical influence on the sediment by plants. However, it is possible
752 that benthic organisms such as worms may have influenced the biogeochemistry in both the pioneer marsh and
753 intertidal flat, causing some variability.

754 4.2.2 Effect of organic carbon input in the pioneer marsh

755 Carbon dioxide fluxes

756 To test our hypothesis that that microbially mediated CO₂ release is OC limited in the pioneer marsh, we
757 injected two different OC sources into the sediment and monitored the subsequent release of CO₂ 1.5, 24, and 48 h post
758 injection. We observed that acetate treated plots emitted the highest CO₂ throughout the experiment (Fig. 4). No
759 difference in the CO₂ release was measured between the humic acid treatment and the control despite the additional
760 availability of OC. This is supported by the work of Gunina and Kuzyakov (2022) who showed that reduced and
761 complex organics in soils are predominantly thermodynamically preserved due to insufficient energy yield upon
762 decomposition. Humic acid, as complex OC, may be thus preserved in our study, as reflected in higher DOC
763 concentrations. In contrast, acetate, with a simpler chemical structure, is favourable for microbial decomposition even
764 under reducing conditions (Boye et al., 2017; LaRowe and Van Cappellen, 2011) and thus could be readily utilized
765 and oxidized to CO₂. Notably, plots treated with humic acid received the same OC concentrations as the acetate plots,
766 indicating that OC composition is crucial for the CO₂ release from minerogenic pioneer marshes. Based on the
767 geochemistry at the field site, which suggested that the ecosystem is limited by the availability of OC, the results from
768 the in situ experiment further support our hypothesis, while simultaneously highlighting the importance of OC
769 composition. This is contrasting to other terrestrial wetlands, which are characterized by a depletion of TEAs
770 (Schlesinger and Bernhardt, 2013b).

771 The increased turnover of acetate to CO₂ relative to humic acid is also evidenced in the DOC concentrations
772 (Fig. S4) and the retention fraction of both DOC sources (Fig. 3a). Although the same mass of OC was added to both
773 treatments, the DOC concentrations in the acetate plots were significantly lower than that in the humic acid plots,

774 suggesting that more acetate was utilized, reflected in higher CO₂ release. However, this result does not explain the
775 lower retention of DOC relative to the retention of Br⁻ from the humic acid plots (Fig. 3a). This suggests that in addition
776 to flushing out, adsorption likely occurred. Previous studies have shown that minerals within the subsurface adsorb
777 organic compounds (Kahle et al., 2003; Kleber et al., 2021). This adsorption may be preferential, favouring more
778 aromatic and high molecular weight compounds, particularly when metal (oxyhydr)oxides and clay minerals are
779 present (Kaiser and Guggenberger, 2000; Lv et al., 2016; Voggenreiter et al., 2024). Based on the results of our study
780 and a previous study conducted at the same site (Kubeneck et al., 2024), both iron(oxyhydr)oxides and clay minerals
781 are present. As adsorption suppresses the decomposition of OC (Kleber et al., 2021), we speculate that the lower
782 retention fraction of humic acid compared to Br⁻ was primarily due to adsorption onto the sediment rather than
783 decomposition. This is consistent with the CO₂ fluxes: humic acid treated plots showed lower retention fractions
784 compared to the Br⁻ retention fractions, however, the CO₂ fluxes were comparable to the control. This suggests that
785 little to no decomposition occurred and that adsorption was the dominant process. It is worth noting that anoxic
786 decomposition of humic acid is generally possible but the turnover time would have exceeded the duration of the
787 experiment (Lipczynska-Kochany, 2018). These results highlight that it is not only the presence of OC that affects
788 short-term OC release from coastal wetlands; the composition of OC is the primary determining factor.

789 [Furthermore, it is important to note that the OC concentrations used in this experiment are higher than those](#)
790 [expected for naturally occurring OC inputs, such as root exudates, which are typically released at lower concentrations](#)
791 [with a continuous input. Thus, upscaling the enhanced CO₂ fluxes measured in our study might result in overestimation](#)
792 [of CO₂ release from minerogenic salt marshes. Our findings rather reveal, on a process level, that the addition of labile](#)
793 [OC stimulates microbially mediated CO₂ release. Enhanced CO₂ release from the acetate amended plots was measured](#)
794 [at nearly all sampling time points \(1.5, 24, and 48 h\) without a clear trend, while the concentration of the inert tracer](#)
795 [showed a slight decrease over the same period \(Fig. S3\) – indicating slight dilution and flushing of the injected OC.](#)
796 [This suggest that the elevated CO₂ release was driven by enhanced availability of labile OC independently of its](#)
797 [concentration. These findings allow us to generalize that the system is likely limited by labile OC availability,](#)
798 [regardless of the concentration; however, further work should quantify how the magnitude of CO₂ promotion](#)
799 [corresponds to OC concentration, particularly under low, naturally sustained OC input rates. In conclusion, we can](#)
800 [reliably predict the direction of increased OC inputs to minerogenic salt marshes, but further studies are needed to](#)
801 [predict the specific long-term magnitude of changes in the carbon cycle in these ecosystems.](#)

802 **Enhanced microbial Fe(III) reduction leads to higher CO₂ release**

803 This section combines the observed effect of OC input on the geochemistry of the porewater and sediment
804 with the microbial growth and metabolic activity and links them to the CO₂ release from the pioneer marsh. The
805 bacterial 16S rRNA gene copy number, an indicator of the total bacterial abundance, was significantly higher in the
806 acetate treatment compared to the control for both DNA and RNA at both depths. This suggests greater bacterial
807 abundance and metabolic activity, which likely led to higher CO₂ fluxes from these plots. No significant difference
808 was noticeable in the 16S rRNA gene copy number between plots amended with humic acid and the control. Overall,
809 the 16S rRNA gene copy numbers (DNA) are in the range of other studies from coastal wetlands and marine sediment
810 (Petro et al., 2019; Zhou et al., 2017).

811 The enhanced metabolic activity in the acetate treated plots is further reflected in the elevated aqueous and
812 solid phase Fe(II). The acetate treatment showed higher aqueous Fe(II) concentrations in all four injection cycles, while
813 no significant difference was observed between the humic acid and control plots. In the solid phase, the Fe(II) content
814 was the highest in the acetate treatment. Thus, the higher expression of *Geobacter* spp. in the acetate treated plots
815 corresponds well to our geochemical observations. *Geobacter* spp. have been shown to use acetate as a carbon source
816 to gain energy (Coates et al., 1996). The higher Fe(II) levels observed in both aqueous and solid phase of acetate treated
817 plots along with elevated *Geobacter* spp. gene copies indicate that Fe(III) reduction was stimulated by increased
818 availability of labile OC.

819 Ferric iron and SO_4^{2-} reduction have been reported as OC decomposition processes in salt marshes (Hyun et
820 al., 2007; Kostka et al., 2002a; Lowe et al., 2000). Sulfide concentrations in the porewater as well as in the solid phase
821 gave evidence that SO_4^{2-} reduction occurred; however, no differences between the treatments and controls were seen.
822 The functional gene analysis provided further evidence for this, as sulfate-reducing bacteria (SRB) were present
823 (absolute gene copy numbers in Supplement, Fig. S7); however, none of the treatments led to an increase in their
824 metabolic activity compared to the control (Fig. 6). Thus, we speculate that the higher CO_2 release from the acetate
825 treatment was mainly driven by the enhanced Fe(III) reduction and not by SO_4^{2-} reduction. Our finding that acetate is
826 utilized follows the conventional thermodynamic sequence of iron reduction being more favorable than SO_4^{2-} reduction
827 (Schlesinger and Bernhardt, 2013b) – even if the concentrations and availability of SO_4^{2-} were much higher.
828

Deleted: lead

Deleted: was

831 **4.2.3 Effect of organic carbon input in the intertidal flat**

832 **Carbon dioxide fluxes**

833 Adding OC to the intertidal flat, a zone more influenced by tides than the pioneer marsh, resulted in CO₂
834 trends similar to the pioneer marsh. Acetate addition led to a noticeable increase in CO₂ fluxes. In contrast, the CO₂
835 fluxes from the humic acid and control plots were similar. This supports our hypothesis that the electron donor limits
836 CO₂ release from the ecosystem. Moreover, it highlights that irrespective of tidal influence, the system is limited by
837 the availability and composition of OC.

838 **Enhanced microbial activity leads to higher CO₂ release**

839 Total microbial 16S gene copies were significantly higher in the acetate treated intertidal flat plots compared
840 to the control at both depths (RNA-based), whereas plots amended with humic acid showed no significant difference
841 from the control plots (Fig. S12a). In contrast to the significant increase in *Geobacter* spp. gene copies, no difference
842 in the aqueous Fe(II) or in the Fe(II) content in the upper sediment layer (0-5 cm) was measured for the acetate
843 treatment, except for a higher Fe(II) content in the deeper sediment layer. Conversely, we measured higher AVS
844 contents in the upper layer for the acetate treatment, but this is not reflected in higher *dsrA* copies numbers. Based on
845 these mixed results, we consider two hypotheses: (i) acetate promoted increased Fe(III) reduction, which is supported
846 by higher gene copies of *Geobacter* spp.. However, this is not clearly reflected in the Fe(II) data. Furthermore, with
847 increased Fe(III) reduction and a constant SO₄²⁻ reduction rate, we would have expected a depletion of S(II)_{tot} in the
848 porewater of the acetate treatment due to iron-sulfur mineral formation; however, this was not observed. Thus, we
849 consider a second hypothesis that (ii) acetate promoted SO₄²⁻ reduction, supported by increased AVS content in the
850 acetate treatment in the upper sediment layer. In contrast, the number of *dsrA* gene copies was not higher in the acetate
851 treatment. Although a small increase (RNA-based) in the gene copies of *dsrA* was observed in the upper layer, this
852 was not statistically significant. Additionally, no differences were observed in the S(II)_{tot} concentrations, which were
853 generally low and should therefore be interpreted with caution. Based on our data, we cannot clearly reject either
854 hypothesis. We therefore suggest Fe(III) and SO₄²⁻ reduction both lead to higher CO₂ release, stimulated by higher
855 supply of labile OC in the intertidal flat.

856 5 Conclusion and Implications

857 Our study demonstrated that the composition in combination with the concentration of OC determines the
858 CO₂ release from minerogenic salt marshes typical of the Wadden Sea. Initial porewater and sediment geochemical
859 characterization indicated that microbially mediated CO₂ release is likely not limited by the availability of electron
860 acceptors in both the pioneer marsh and intertidal flat, contrary to what is generally observed in terrestrial wetlands.
861 [We caution here that we did not directly measure TEA reduction rates. Future studies should investigate turnover rates,](#)
862 [potentially utilizing isotopes to confirm this finding. Overall, our results indicate that the OC composition, rather than](#)
863 [the concentration alone, controlled CO₂ release in both succession zones. This suggests that OC composition likely](#)
864 [plays a limiting role in microbially mediated CO₂ release from minerogenic salt marshes.](#) The higher CO₂ release
865 observed in the acetate treated plots within the pioneer marsh was accompanied by higher levels of reduced iron. This
866 pattern also corresponded with greater activity of Fe(III)-reducing bacteria in these plots, indicating that microbially
867 mediated CO₂ release resulted from Fe(III) reduction driven by increased labile OC input. The addition of the complex
868 OC (humic acid) did not exceed the CO₂ release of the control, showing that complex OC was not decomposed. Overall,
869 our results indicate that the OC composition, rather than the concentration alone, limits the CO₂ release from
870 minerogenic salt marshes. Similar trends in CO₂ release were measured for the intertidal flat, further indicating that
871 OC (both in terms of composition and concentration) is the key driver of microbial decomposition of OC to CO₂ for
872 salt marsh systems. We expect that this is particularly relevant in salt marshes similar to ours with a high proportion
873 of fine particles (muddy marshes) relative to marshes with larger particles (sandy marshes).

874 The results of this in situ study contribute to our understanding of [short-term](#) carbon dynamics in minerogenic
875 temperate salt marshes. Labile OC inputs such as root exudates may enhance CO₂ release from minerogenic salt
876 marshes, while complex OC inputs, such as plant fragments, might be sequestered in the sediment rather than degraded
877 and released as CO₂. The controls on OC turnover observed here should be considered when accounting for these
878 ecosystems as carbon sinks and stocks. Also, our results show that the link between OC composition and the release
879 of CO₂, independent of electron acceptor concentrations, is crucial and should be included in process-based modelling
880 of carbon fluxes in these ecosystems (Brown, 2025; Regnier et al., 2013). This will contribute to more accurate
881 predictions of the response of salt marshes to climate change. Further, the in situ experiment simulated a potential
882 increase [of short-term](#) OC inputs to the ecosystem, reflecting scenarios associated with climate change such as
883 inundation of previously unflooded areas due to sea level rise and storm surges or eutrophication (van Beusekom,
884 2005; Esselink et al., 2017; Woth et al., 2006). For example, eutrophication may result in an input of organic matter
885 into the Wadden Sea that is eventually washed onto the coastal sediment. Our study thus provides valuable insight into
886 the consequences of such [short-term](#) scenarios for GHG release and highlights that the input of labile OC (e.g., primary
887 production during eutrophication, root exudates) into the sediment of a minerogenic salt marsh results in higher CO₂
888 releases.

Deleted: From the in situ manipulation experiment, we observed that both succession zones were sensitive to labile OC input. ...

Deleted: in

893 **CRedit authorship contribution statement**

894 **NK:** Investigation, Methodology, Formal Analysis, Visualization, Writing – Original Draft Preparation,
895 Conceptualization. **FR:** Investigation, Writing – Review & Editing. **LJK:** Methodology, Writing – Review & Editing.
896 **RK:** Methodology, Writing – Review & Editing. **AK:** Writing – Review & Editing, Funding Acquisition. **PJ:**
897 Conceptualization, Funding Acquisition, Supervision, Project Administration, Writing – Review & Editing.

Deleted: Nora Kainz

Deleted: Franziska Raab

Deleted: Joëlle Kubeneck

Deleted: Ruben Kretzschmar

Deleted: Andreas Kappler

Deleted: Prachi Joshi

898 **Competing interests**

899 The authors declare that they have no conflict of interest.

900 **Acknowledgements**

901 PJ would like to thank the Ministerium für Wissenschaft, Forschung und Kunst Baden-Württemberg, the University
902 of Tübingen, and the Deutsche Forschungsgemeinschaft (DFG) for funding through the program Projektförderung für
903 NachwuchswissenschaftlerInnen. We are grateful for financial support from the Deutsche Forschungsgemeinschaft
904 (DFG, German Research Foundation, project ID 431072007) and for infrastructural support by the DFG under
905 Germany's Excellence Strategy, cluster of Excellence EXC2124 (project ID 390838134). LJK and RK were funded
906 by the European Research Council (ERC) under the European Union's Horizon 2020 research and innovation program
907 (grant agreement no. 788009-IRMIDYN-ERC-2017-ADG). Furthermore, the authors gratefully acknowledge the
908 Landesbetrieb für Küstenschutz, Nationalpark und Meeresschutz Schleswig-Holstein and the Nationalpark
909 Wattenmeer Schleswig-Holstein for permission to conduct our work. For wording and rephrasing in some sections of
910 the article, an artificial intelligence tool (ChatGPT) was used. We used BioRender to illustrate the experimental setup;
911 we appreciate their tool. Many thanks to all students, especially to Johanna Isele and Franziska Heitmann, for their
912 help in the field and laboratory. We are also grateful to Franziska Schädler for her assistance with the molecular biology
913 analysis. We would like to thank Muammar Mansor for help in the field as well as useful discussions.

914 **Data availability statement**

915 Data are publicly available at Zenodo via doi.org/10.5281/zenodo.17136252 (Kainz et al., 2025)

922 **References**

- 923 Alongi, D. M.: Carbon Balance in Salt Marsh and Mangrove Ecosystems: A Global Synthesis, *Journal of*
924 *Marine Science and Engineering*, 8, 1–21, <https://doi.org/10.3390/jmse8100767>, 2020.
- 925 Arndt, S., Jørgensen, B. B., LaRowe, D. E., Middelburg, J. J., Pancost, R. D., and Regnier, P.: Quantifying
926 the degradation of organic matter in marine sediments: A review and synthesis, *Earth-Science Reviews*,
927 123, 53–86, <https://doi.org/10.1016/j.earscirev.2013.02.008>, 2013.
- 928 de Beer, D., Wenzhöfer, F., Ferdelman, T. G., Boehme, S. E., Huettel, M., Van Beusekom, J. E. E., Böttcher,
929 M. E., Musat, N., and Dubilier, N.: Transport and mineralization rates in North Sea sandy intertidal
930 sediments, Sylt-Rømø Basin, Wadden Sea, *Limnology and Oceanography*, 50, 113–127,
931 <https://doi.org/10.4319/lo.2005.50.1.0113>, 2005.
- 932 van Beusekom, J. E. E.: A historic perspective on Wadden Sea eutrophication, *Helgoland Marine*
933 *Research*, 59, 45–54, <https://doi.org/10.1007/s10152-004-0206-2>, 2005.
- 934 Bosselmann, K., Böttcher, M. E., Billerbeck, M., Walpersdorf, E., Theune, A., Huettel, M., and Jørgensen,
935 B. B.: Iron-Sulfur-Manganese Dynamics in Intertidal Surface Sediments of the North Sea, *Berichte -*
936 *Forschungszentrum Terramare*, 32–35, 2003.
- 937 Boye, K., Noël, V., Tfaily, M. M., Bone, S. E., Williams, K. H., Bargar, J. R., and Fendorf, S.:
938 Thermodynamically controlled preservation of organic carbon in floodplains, *Nature Geoscience*, 10,
939 415–419, <https://doi.org/10.1038/ngeo2940>, 2017.
- 940 Brown, C. J.: Simulated Biogeochemical Effects of Seawater Restoration on Diked Salt Marshes, Cape Cod
941 National Seashore, Massachusetts, U.S., *Soil Systems*, 9, 89,
942 <https://doi.org/10.3390/soilsystems9030089>, 2025.
- 943 BSH: Federal Maritime and Hydrographic Agency, *Gezeiten [Dataset]*. Bundesamt für Seeschifffahrt und
944 Hydrographie, Hamburg and Rostock, Germany, 2025.
- 945 Burton, E. D., Bush, R. T., Sullivan, L. A., and Mitchell, D. R. G.: Reductive transformation of iron and
946 sulfur in schwertmannite-rich accumulations associated with acidified coastal lowlands, *Geochimica et*
947 *Cosmochimica Acta*, 71, 4456–4473, <https://doi.org/10.1016/j.gca.2007.07.007>, 2007.
- 948 Capocci, M., Seyfferth, A. L., Tobias, C., Wozniak, A. S., Hedgpeth, A., Bowen, M., Biddle, J. F., McFarlane,
949 K. J., and Vargas, R.: High methane concentrations in tidal salt marsh soils: Where does the methane go?,
950 *Global Change Biology*, 30, 1–19, <https://doi.org/10.1111/gcb.17050>, 2024.
- 951 Cline, J. D.: Spectrophotometric Determination of Hydrogen Sulfide in Natural Waters, *Limnology and*
952 *Oceanography*, 14, 454–458, <https://doi.org/10.4319/lo.1969.14.3.0454>, 1969.
- 953 Coates, J. D., Phillips, E. J., Lonergan, D. J., Jenter, H., and Lovley, D. R.: Isolation of *Geobacter* species
954 from diverse sedimentary environments, *Applied and Environmental Microbiology*, 62, 1531–1536,
955 <https://doi.org/10.1128/aem.62.5.1531-1536.1996>, 1996.
- 956 Common Wadden Sea Secretariat: Wadden Sea Quality Status Report: Introduction, Common Wadden
957 Sea Secretariat, <https://doi.org/10.5281/ZENODO.15195139>, 2017.

Formatted: German

958 Cornwell, J. C. and Morse, J. W.: The characterization of iron sulfide minerals in anoxic marine sediments,
959 *Marine Chemistry*, 22, 193–206, [https://doi.org/10.1016/0304-4203\(87\)90008-9](https://doi.org/10.1016/0304-4203(87)90008-9), 1987.

960 Duarte, C. M., Middelburg, J. J., and Caraco, N.: Major role of marine vegetation on the oceanic carbon
961 cycle, *Biogeosciences*, 2, 1–8, <https://doi.org/10.5194/bg-2-1-2005>, 2005.

962 Duarte, C. M., Dennison, W. C., Orth, R. J. W., and Carruthers, T. J. B.: The charisma of coastal
963 ecosystems: Addressing the imbalance, *Estuaries and Coasts*: J CERF, 31, 233–238,
964 <https://doi.org/10.1007/s12237-008-9038-7>, 2008.

965 Duarte, C. M., Losada, I. J., Hendriks, I. E., Mazarrasa, I., and Marbà, N.: The role of coastal plant
966 communities for climate change mitigation and adaptation, *Nature Climate Change*, 3, 961–968,
967 <https://doi.org/10.1038/nclimate1970>, 2013.

968 van Erk, M. R., Bourceau, O. M., Moncada, C., Basu, S., Hansel, C. M., and De Beer, D.: Reactive oxygen
969 species affect the potential for mineralization processes in permeable intertidal flats, *Nature*
970 *Communications*, 14, 938, <https://doi.org/10.1038/s41467-023-35818-4>, 2023.

971 Esselink, P., van Duin, W. E., Bunje, J., Cremer, J., Folmer, E. O., Frikke, J., Glahn, M., de Groot, A. V.,
972 Hecker, N., Hellwig, U., Jensen, K., Körber, P., Petersen, J., and Stock, M.: Salt marshes. In: Wadden Sea
973 Quality Status Report 2017, Common Wadden Sea Secretariat, Wilhelmshaven, Germany. Downloaded
974 03.11.2024. qsr.waddensea-worldheritage.org/reports/salt-marshes, 2017.

975 Gao, S.: Chapter 10: Geomorphology and Sedimentology of Tidal Flats, in: In: Coastal Wetlands (Second
976 Edition), *Elsevier*, 359–381, <https://doi.org/10.1016/B978-0-444-63893-9.00010-1>, 2019.

977 Gribsholt, B. and Kristensen, E.: Benthic metabolism and sulfur cycling along an inundation gradient in a
978 tidal *Spartina anglica* salt marsh, *Limnology and Oceanography*, 48, 2151–2162,
979 <https://doi.org/10.4319/lo.2003.48.6.2151>, 2003.

980 Gunina, A. and Kuzyakov, Y.: From energy to (soil organic) matter, *Global Change Biology*, 28, 2169–
981 2182, <https://doi.org/10.1111/gcb.16071>, 2022.

982 Hansen, K., Butzeck, C., Eschenbach, A., Gröngröft, A., Jensen, K., and Pfeiffer, E.-M.: Factors influencing
983 the organic carbon pools in tidal marsh soils of the Elbe estuary (Germany), *Journal of Soils and*
984 *Sediments*, 17, 47–60, <https://doi.org/10.1007/s11368-016-1500-8>, 2017.

985 Heron, G., Crouzet, C., Bourg, A. C. M., and Christensen, T. H.: Speciation of Fe(II) and Fe(III) in
986 Contaminated Aquifer Sediments Using Chemical Extraction Techniques, *Environmental Science &*
987 *Technology*, 28, 1698–1705, <https://doi.org/10.1021/es00058a023>, 1994.

988 Howard, J., Sutton-Grier, A. E., Smart, L. S., Lopes, C. C., Hamilton, J., Kleypas, J., Simpson, S., McGowan,
989 J., Pessarrodona, A., Alleway, H. K., and Landis, E.: Blue carbon pathways for climate mitigation: Known,
990 emerging and unlikely, *Marine Policy*, 156, 105788, <https://doi.org/10.1016/j.marpol.2023.105788>, 2023.

991 Huettel, M., Berg, P., and Kostka, J. E.: Benthic Exchange and Biogeochemical Cycling in Permeable
992 Sediments, *Annual Review of Marine Science*, 6, 23–51, <https://doi.org/10.1146/annurev-marine-051413-012706>, 2014.

Formatted: German

994 Hyun, J.-H., Smith, A. C., and Kostka, J. E.: Relative contributions of sulfate- and iron(III) reduction to
995 organic matter mineralization and process controls in contrasting habitats of the Georgia saltmarsh,
996 *Applied Geochemistry*, 22, 2637–2651, <https://doi.org/10.1016/j.apgeochem.2007.06.005>, 2007.

997 Jørgensen, B. B., Findlay, A. J., and Pellerin, A.: The Biogeochemical Sulfur Cycle of Marine Sediments,
998 *Frontiers in Microbiology*, 10, 1–27, <https://doi.org/10.3389/fmicb.2019.00849>, 2019.

999 Kahle, M., Kleber, M., and Jahn, R.: Retention of dissolved organic matter by illitic soils and clay fractions:
1000 Influence of mineral phase properties, *Journal of Plant Nutrition and Soil Science*, 166, 737–741,
1001 <https://doi.org/10.1002/jpln.200321125>, 2003.

1002 Kainz, N., Raab, F., Kubeneck, L. J., Kretzschmar, R., Kappler, A., and Joshi, P.: Carbon dioxide release
1003 driven by organic carbon in minerogenic salt marshes, <https://zenodo.org/records/17136252>, 2025.

1004 Kaiser, K. and Guggenberger, G.: The role of DOM sorption to mineral surfaces in the preservation of
1005 organic matter in soils, *Organic Geochemistry*, 31, 711–725, [https://doi.org/10.1016/S0146-](https://doi.org/10.1016/S0146-6380(00)00046-2)
1006 [6380\(00\)00046-2](https://doi.org/10.1016/S0146-6380(00)00046-2), 2000.

1007 Kleber, M., Bourg, I. C., Coward, E. K., Hansel, C. M., Myneni, S. C. B., and Nunan, N.: Dynamic
1008 interactions at the mineral–organic matter interface, *Nature Reviews Earth & Environment*, 2, 402–421,
1009 <https://doi.org/10.1038/s43017-021-00162-y>, 2021.

1010 Koop-Jakobsen, K., Fischer, J., and Wenzhöfer, F.: Survey of sediment oxygenation in rhizospheres of the
1011 saltmarsh grass - *Spartina anglica*, *Science of The Total Environment*, 589, 191–199,
1012 <https://doi.org/10.1016/j.scitotenv.2017.02.147>, 2017.

1013 Kostka, J. E., Roychoudhury, A., and Cappellen, V.: Rates and controls of anaerobic microbial respiration
1014 across spatial and temporal gradients in saltmarsh sediments, *Biogeochemistry*, 60, 49–76,
1015 <https://doi.org/10.1023/A:1016525216426>, 2002a.

1016 Kostka, J. E., Gribsholt, B., Petrie, E., Dalton, D., Skelton, H., and Kristensen, E.: The rates and pathways of
1017 carbon oxidation in bioturbated saltmarsh sediments, *Limnology and Oceanography*, 47, 230–240,
1018 <https://doi.org/10.4319/lo.2002.47.1.0230>, 2002b.

1019 Kubeneck, L. J., Notini, L., Rothwell, K. A., Fantappiè, G., Huthwelker, T., ThomasArrigo, L. K., and
1020 Kretzschmar, R.: Transformation of vivianite in intertidal sediments with contrasting sulfide conditions,
1021 *Geochimica et Cosmochimica Acta*, 370, 173–187, <https://doi.org/10.1016/j.gca.2024.01.020>, 2024.

1022 Kubeneck, L. J., Rothwell, K. A., Notini, L., ThomasArrigo, L. K., Schulz, K., Fantappiè, G., Joshi, P.,
1023 Huthwelker, T., and Kretzschmar, R.: In Situ Vivianite Formation in Intertidal Sediments: Ferrihydrite-
1024 Adsorbed P Triggers Vivianite Formation, *Environmental Science & Technology*, 59, 523–532,
1025 <https://doi.org/10.1021/acs.est.4c10710>, 2025.

1026 Kvale, E. P.: The origin of neap–spring tidal cycles, *Marine Geology*, 235, 5–18,
1027 <https://doi.org/10.1016/j.margeo.2006.10.001>, 2006.

1028 La, W., Han, X., Liu, C.-Q., Ding, H., Liu, M., Sun, F., Li, S., and Lang, Y.: Sulfate concentrations affect
1029 sulfate reduction pathways and methane consumption in coastal wetlands, *Water Research*, 217,
1030 118441, <https://doi.org/10.1016/j.watres.2022.118441>, 2022.

- 1031 LaRowe, D. E. and Van Cappellen, P.: Degradation of natural organic matter: A thermodynamic analysis,
1032 *Geochimica et Cosmochimica Acta*, 75, 2030–2042, <https://doi.org/10.1016/j.gca.2011.01.020>, 2011.
- 1033 Lipczynska-Kochany, E.: Humic substances, their microbial interactions and effects on biological
1034 transformations of organic pollutants in water and soil: A review, *Chemosphere*, 202, 420–437,
1035 <https://doi.org/10.1016/j.chemosphere.2018.03.104>, 2018.
- 1036 Llobet-Brossa, E., Rabus, R., Böttcher, M., Könneke, M., Finke, N., Schramm, A., Meyer, R., Grötzschel, S.,
1037 Rosselló-Mora, R., and Amann, R.: Community structure and activity of sulfate-reducing bacteria in an
1038 intertidal surface sediment: a multi-method approach, *Aquatic Microbial Ecology*, 29, 211–226,
1039 <https://doi.org/10.3354/ame029211>, 2002.
- 1040 Logemann, E. L., Goesele, C., Jensen, K., and Mueller, P.: Soil Organic Carbon Stocks of German Salt
1041 Marshes: A Comparative Study Along Low- and High-Energy Coastlines, *JGR Biogeosciences*, 130,
1042 e2025JG008797, <https://doi.org/10.1029/2025JG008797>, 2025.
- 1043 Lowe, K. L., Dichristina, T. J., Roychoudhury, A. N., and Van Cappellen, P.: Microbiological and
1044 Geochemical Characterization of Microbial Fe(III) Reduction in Salt Marsh Sediments, *Geomicrobiology
1045 Journal*, 17, 163–178, <https://doi.org/10.1080/01490450050023836>, 2000.
- 1046 Lueder, U., Maisch, M., Laufer, K., Joørgensen, B. B., Kappler, A., and Schmidt, C.: Influence of Physical
1047 Perturbation on Fe(II) Supply in Coastal Marine Sediments, *Environmental Science & Technology*, 54,
1048 3209–3218, <https://doi.org/10.1021/acs.est.9b06278>, 2020.
- 1049 Lueders, T., Manefield, M., and Friedrich, M. W.: Enhanced sensitivity of DNA- and rRNA-based stable
1050 isotope probing by fractionation and quantitative analysis of isopycnic centrifugation gradients,
1051 *Environmental Microbiology*, 6, 73–78, <https://doi.org/10.1046/j.1462-2920.2003.00536.x>, 2004.
- 1052 Lv, J., Zhang, S., Wang, S., Luo, L., Cao, D., and Christie, P.: Molecular-Scale Investigation with ESI-FT-ICR-
1053 MS on Fractionation of Dissolved Organic Matter Induced by Adsorption on Iron Oxyhydroxides,
1054 *Environmental Science & Technology*, 50, 2328–2336, <https://doi.org/10.1021/acs.est.5b04996>, 2016.
- 1055 Maricle, B. R. and Lee, R. W.: Aerenchyma development and oxygen transport in the estuarine
1056 cordgrasses *Spartina alterniflora* and *S. anglica*, *Aquatic Botany*, 74, 109–120,
1057 [https://doi.org/10.1016/S0304-3770\(02\)00051-7](https://doi.org/10.1016/S0304-3770(02)00051-7), 2002.
- 1058 Martens, C. S. and Berner, R. A.: Methane Production in the Interstitial Waters of Sulfate-Depleted
1059 Marine Sediments, *Science*, 185(4157), 1167–1169, 1974.
- 1060 Mcleod, E., Chmura, G. L., Bouillon, S., Salm, R., Björk, M., Duarte, C. M., Lovelock, C. E., Schlesinger, W.
1061 H., and Silliman, B. R.: A blueprint for blue carbon: Toward an improved understanding of the role of
1062 vegetated coastal habitats in sequestering CO₂, *Frontiers in Ecology and the Environment*, 9, 552–560,
1063 <https://doi.org/10.1890/110004>, 2011.
- 1064 Moeslund, L., Thamdrup, B., and Barker Jørgensen, B.: Sulfur and iron cycling in a coastal sediment:
1065 Radiotracer studies and seasonal dynamics, *Biogeochemistry*, 27, 129–152,
1066 <https://doi.org/10.1007/BF00002815>, 1994.

- 1067 Mueller, P., Ladiges, N., Jack, A., Schmiel, G., Kutzbach, L., Jensen, K., and Nolte, S.: Assessing the long-
1068 term carbon-sequestration potential of the semi-natural salt marshes in the European Wadden Sea,
1069 *Ecosphere*, 10, <https://doi.org/10.1002/ecs2.2556>, 2019.
- 1070 Mueller, P., Kutzbach, L., Mozdzer, T. J., Jespersen, E., Barber, D. C., and Eller, F.: Minerogenic salt
1071 marshes can function as important inorganic carbon stores, *Limnology and Oceanography*, 68, 942–952,
1072 <https://doi.org/10.1002/lno.12322>, 2023.
- 1073 Nellemann, C., Corcoran, E., Duarte, C. M., Valdés, L., De Young, C., Fonseca, L., and Grimsditch, G.: Blue
1074 Carbon - The Role of Healthy Oceans in Binding Carbon, UNEP. ISBN: 978-82-7701-060-1, 80 pp., 2009.
- 1075 Nolte, S., Koppelaar, E. C., Esselink, P., Dijkema, K. S., Schuerch, M., De Groot, A. V., Bakker, J. P., and
1076 Temmerman, S.: Measuring sedimentation in tidal marshes: a review on methods and their applicability
1077 in biogeomorphological studies, *Journal of Coastal Conservation*, 17, 301–325,
1078 <https://doi.org/10.1007/s11852-013-0238-3>, 2013.
- 1079 Novák, V. and Hlaváčková, H.: Soil-Water Movement in Water-Saturated Capillary Porous Media, in:
1080 Applied Soil Hydrology, vol. 32, Springer International Publishing, Cham, 97–117,
1081 https://doi.org/10.1007/978-3-030-01806-1_8, 2019.
- 1082 Pendleton, L., Donato, D. C., Murray, B. C., Crooks, S., Jenkins, W. A., Sifleet, S., Craft, C., Fourqurean, J.
1083 W., Kauffman, J. B., Marbà, N., Megonigal, P., Pidgeon, E., Herr, D., Gordon, D., and Baldera, A.:
1084 Estimating Global “Blue Carbon” Emissions from Conversion and Degradation of Vegetated Coastal
1085 Ecosystems, *PLoS ONE*, 7, e43542, <https://doi.org/10.1371/journal.pone.0043542>, 2012.
- 1086 Petro, C., Zäncker, B., Starnawski, P., Jochum, L. M., Ferdelman, T. G., Jørgensen, B. B., Røy, H., Kjeldsen,
1087 K. U., and Schramm, A.: Marine Deep Biosphere Microbial Communities Assemble in Near-Surface
1088 Sediments in Aarhus Bay, *Frontiers in Microbiology*, 10, 758, <https://doi.org/10.3389/fmicb.2019.00758>,
1089 2019.
- 1090 Poffenbarger, H. J., Needelman, B. A., and Megonigal, J. P.: Salinity Influence on Methane Emissions from
1091 Tidal Marshes, *Wetlands*, 31, 831–842, <https://doi.org/10.1007/s13157-011-0197-0>, 2011.
- 1092 Regnier, P., Arndt, S., Goossens, N., Volta, C., Laruelle, G. G., Lauerwald, R., and Hartmann, J.: Modelling
1093 Estuarine Biogeochemical Dynamics: From the Local to the Global Scale, *Aquatic Geochemistry*, 19, 591–
1094 626, <https://doi.org/10.1007/s10498-013-9218-3>, 2013.
- 1095 Revsbech, N. P.: An oxygen microsensor with a guard cathode, *Limnology and Oceanography*, 34, 474–
1096 478, <https://doi.org/10.4319/lo.1989.34.2.0474>, 1989.
- 1097 Røy, H., Lee, J. S., Jansen, S., and De Beer, D.: Tide-driven deep pore-water flow in intertidal sand flats,
1098 *Limnology and Oceanography*, 53, 1521–1530, <https://doi.org/10.4319/lo.2008.53.4.1521>, 2008.
- 1099 Schlesinger, W. H. and Bernhardt, E. S.: Chapter 5: The Biosphere: The Carbon Cycle of Terrestrial
1100 Ecosystems, in: Biogeochemistry (3rd edition), Elsevier, Waltham, MA, USA, 135–172,
1101 <https://doi.org/10.1016/B978-0-12-385874-0.00005-4>, 2013a.
- 1102 Schlesinger, W. H. and Bernhardt, E. S.: Chapter 7: Wetland Ecosystems, in: Biogeochemistry (3rd
1103 edition), Elsevier, Waltham, MA, USA, 233–274, <https://doi.org/10.1016/B978-0-12-385874-0.00007-8>,
1104 2013b.

- 1105 Seyfferth, A. L., Bothfeld, F., Vargas, R., Stuckey, J. W., Wang, J., Kearns, K., Michael, H. A., Guimond, J.,
 1106 Yu, X., and Sparks, D. L.: Spatial and temporal heterogeneity of geochemical controls on carbon cycling in
 1107 a tidal salt marsh, *Geochimica et Cosmochimica Acta*, 282, 1–18,
 1108 <https://doi.org/10.1016/j.gca.2020.05.013>, 2020.
- 1109 Stookey, L. L.: Ferrozine-a new spectrophotometric reagent for iron, *Analytical Chemistry*, 42, 779–781,
 1110 <https://doi.org/10.1021/ac60289a016>, 1970.
- 1111 Tan, J. H. Y., Mosley, L. M., and Wong, V. N. L.: A Review of Fe–S–C Dynamics in Blue Carbon
 1112 Environments: Potential Influence of Coastal Acid Sulfate Soils, *European Journal of Soil Science*, 76,
 1113 e70047, <https://doi.org/10.1111/ejss.70047>, 2025.
- 1114 Temmink, R., J. M., Lamers, L. P. M., Angelini, C., Bouma, T. J., Fritz, C., van de Koppel, J., Lexmond, R.,
 1115 Rietkerk, M., Silliman, B. R., Joosten, H., and van der Heide, T.: Recovering wetland biogeomorphic
 1116 feedbacks to restore the world’s biotic carbon hotspots, *Science*, 376, 1–7,
 1117 <https://doi.org/doi.org/10.1126/science.abn1479>, 2022.
- 1118 Tobias, C. and Neubauer, S. C.: Salt Marsh Biogeochemistry - An Overview, in: Coastal Wetlands: An
 1119 Integrated Ecosystem Approach, vol. Chapter 16, *Elsevier*, 539–596, [https://doi.org/10.1016/B978-0-444-](https://doi.org/10.1016/B978-0-444-63893-9.00016-2)
 1120 [63893-9.00016-2](https://doi.org/10.1016/B978-0-444-63893-9.00016-2), 2019.
- 1121 Trifunovic, B., Vázquez-Lule, A., Capooci, M., Seyfferth, A. L., Moffat, C., and Vargas, R.: Carbon Dioxide
 1122 and Methane Emissions From A Temperate Salt Marsh Tidal Creek, *Journal of Geophysical Research:*
 1123 *Biogeosciences*, 125, e2019JG005558, <https://doi.org/10.1029/2019JG005558>, 2020.
- 1124 Van de Broek, M., Vandendriessche, C., Poppelmonde, D., Merckx, R., Temmerman, S., and Govers, G.:
 1125 Long-term organic carbon sequestration in tidal marsh sediments is dominated by old-aged
 1126 allochthonous inputs in a macrotidal estuary, *Global Change Biology*, 24, 2498–2512,
 1127 <https://doi.org/10.1111/gcb.14089>, 2018.
- 1128 de Vlas, J., Mandema, F., Nolte, S., van Klink, R., and Esselink, P.: Nature conservation of salt marshes.
 1129 The influence of grazing on biodiversity, PUCCIMAR report 09., It Fryske Gea, Olterterp, 2013.
- 1130 Voggenreiter, E., Schmitt-Kopplin, P., Thomas Arrigo, L., Bryce, C., Kappler, A., and Joshi, P.: Emerging
 1131 investigator series: preferential adsorption and coprecipitation of permafrost organic matter with poorly
 1132 crystalline iron minerals, *Environmental Science: Processes & Impacts*, 26, 1322–1335,
 1133 <https://doi.org/10.1039/D4EM00241E>, 2024.
- 1134 Wang, J., Hua, M., Cai, C., Hu, J., Wang, J., Yang, H., Ma, F., Qian, H., Zheng, P., and Hu, B.: Spatial-
 1135 Temporal Pattern of Sulfate-Dependent Anaerobic Methane Oxidation in an Intertidal Zone of the East
 1136 China Sea, *Applied and Environmental Microbiology*, 85, e02638-18,
 1137 <https://doi.org/10.1128/AEM.02638-18>, 2019.
- 1138 Woth, K., Weisse, R., and Von Storch, H.: Climate change and North Sea storm surge extremes: an
 1139 ensemble study of storm surge extremes expected in a changed climate projected by four different
 1140 regional climate models, *Ocean Dynamics*, 56, 3–15, <https://doi.org/10.1007/s10236-005-0024-3>, 2006.
- 1141 Wu, C. S., Røy, H., and De Beer, D.: Methanogenesis in sediments of an intertidal sand flat in the Wadden
 1142 Sea, *Estuarine, Coastal and Shelf Science*, 164, 39–45, <https://doi.org/10.1016/j.ecss.2015.06.031>, 2015.

1143 Zhou, Z., Meng, H., Liu, Y., Gu, J.-D., and Li, M.: Stratified Bacterial and Archaeal Community in Mangrove
1144 and Intertidal Wetland Mudflats Revealed by High Throughput 16S rRNA Gene Sequencing, *Frontiers in*
1145 *Microbiology*, 8, 2148, <https://doi.org/10.3389/fmicb.2017.02148>, 2017.

1146